UNIVERSITA' DEGLI STUDI DI PADOVA

FACOLTA DI SCIENZE MM. FF. NN.
Dipartimento di Geoscienze
Direttore Prof. Cristina Stefani

TESI DI LAUREA MAGISTRALE
IN
GEOLOGIA E GEOLOGIA TECNICA

ANALYSIS OF THE CENOZOIC EXHUMATION IN THE BARENTS SEA WITH THERMOCHRONOLOGICAL METHODS

Relatore: *Prof. Massimiliano Zattin*
Correlatori: *Dr. Domenico Grigo*
Dr. Benedetta Andreucci

Laureando: *Barbara De Toffoli*

ANNO ACCADEMICO 2014/2015

TABLE OF CONTENTS

RIASSUNTO

L’area del mare di Barents, parte del territorio offshore della Norvegia, possiede caratteristiche che la rendono uno dei principali target europei per l’esplorazione petrolifera. Mediante l’uso congiunto di tecniche basate sulla geo-termocronologia e di programmi per lo sviluppo della storia termica, è stata ricostruita l’evoluzione che quest’area ha affrontato negli ultimi milioni di anni. Nella fattispecie è stato applicato il metodo (U-Th)/He su apatite, che consente di studiare in dettaglio l’evoluzione termica a basse temperature (<100°C). I campioni, provenienti da carote prelevate da alcuni pozzi situati nella porzione sud-occidentale del mare di Barents, sono stati lavorati e trattati al fine di estrarre i minerali utili per lo svolgimento delle analisi. Dopo la misurazione delle quantità di U, Th ed He, i dati ottenuti sono stati utilizzati per identificare l’età del più recente evento di esumazione avvenuto nell’area e chiarire quelle che ne furono le cause. I dati ottenuti da questo studio suggeriscono che l’esumazione sia legata a cause di tipo tettonico e non da mettere in relazione, come sostenuto da alcuni Autori, alle dinamiche glaciali pleistoceniche. L’individuazione e lo studio di eventi di questo tipo sono di fondamentale importanza per la valutazione delle problematiche legate all’esplorazione petrolifera e alla messa in produzione di pozzi per l’estrazione di idrocarburi.

ABSTRACT

The Barents Sea area, located in the offshore Nowegian territory, is one of the main European target for petroleum exploration. By means of geo-thermochronology techniques and software that can elaborate thermal histories, Cenozoic evolution of the area has been reconstructed. Specifically the (U-Th)/He method on apatites has been applied in order to evaluate the thermal evolution of rocks al low temperatures (<100°C). Samples, from well's cores situated in the south-western Barents Sea, were crushed and treated to extract crystals suitable for the analysis. Measured ages were then used to identify the specific timing of the very last exhumation in the area and which were the causes of the event. Data suggest that the last Barents Sea exhumation has to be related to tectonic causes and not to Pleistocene glacial dynamics, as indicated by some literature. The study of these events play a key role in the hydrocarbon exploration and in the evaluation of risk connected to petroleum plays production.

CHAPTER 1

INTRODUCTION

The aim of this study is to discuss the Cenozoic tectonic evolution of the southern Barents Sea through thermochronological analysis. The area considered for this work is located in the Norwegian offshore territory, in the region of the shelf open to hydrocarbon exploration, whose extent is of about 230.000 km^2. The Norwegian shelf is not the only area, in the Arctic region, where petroleum exploration has a remarkable importance. Beyond the Barents Sea there are many exploration and production sites all over the circumpolar region, involving the shelf around Canada, Greenland, Alaska and Siberia (Dorè, 1995).

Reconstruction of tectonic evolution is crucial for the evaluation of formation and preservation of petroleum plays. In fact, effects related to the occurrence of tectonic events could be: spillage from traps, variation of the overload producing seals failures, removal of confining pressure with a consequent loss of oil and gas resources or modifications of the thermal asset which could influence the generation capacity of the source rock (Dorè et al., 1999). It is noteworthy that there are many examples of preserved petroleum systems even if affected by tectonics which, in some cases, could lead to positive effects such as a reduction of pressure, that, in turn, could better preserve gas and condensate (Green and Duddy, 2010). Nevertheless previous studies classified the south-western Barents Sea as a low risk area for exploration, as most of the shelf as shown in figure 1.1 (b,c). In south-western Barents Sea, where the study area is located, there are seven petroleum plays (Cavanagh et al., 2014). The oldest three are estimated to be in Permian-Carboniferous karstified carbonate strata (Henriksen et al., 2011), the other four plays are Mesozoic and Cenozoic (Cavanagh et al., 2014). The importance of accurate and enhanced studies is accounted for the rich volumes of resources stored beneath the Barents Sea seafloor, particularly from high-quality Triassic sources of the south-west (Henriksen et al., 2011). However, despite the

potential of hydrocarbons and the good discovery rate, just a few of the findings are suitable for commercial purposes. Given the inferred generated volumes of hydrocarbons, it is reasonable to suppose that late events caused significant spillage from traps (Henriksen et al., 2011).

The study aims to the reconstruction of the tectonic evolution of the area focusing on the late Cenozoic events. In this work, the issue will be handled by using quantitative analysis in order to lead to an accurate estimation of exhumation timing. By using appropriate thermochronological methods, models of the thermal history have been performed in order to clarify the last tectonic.

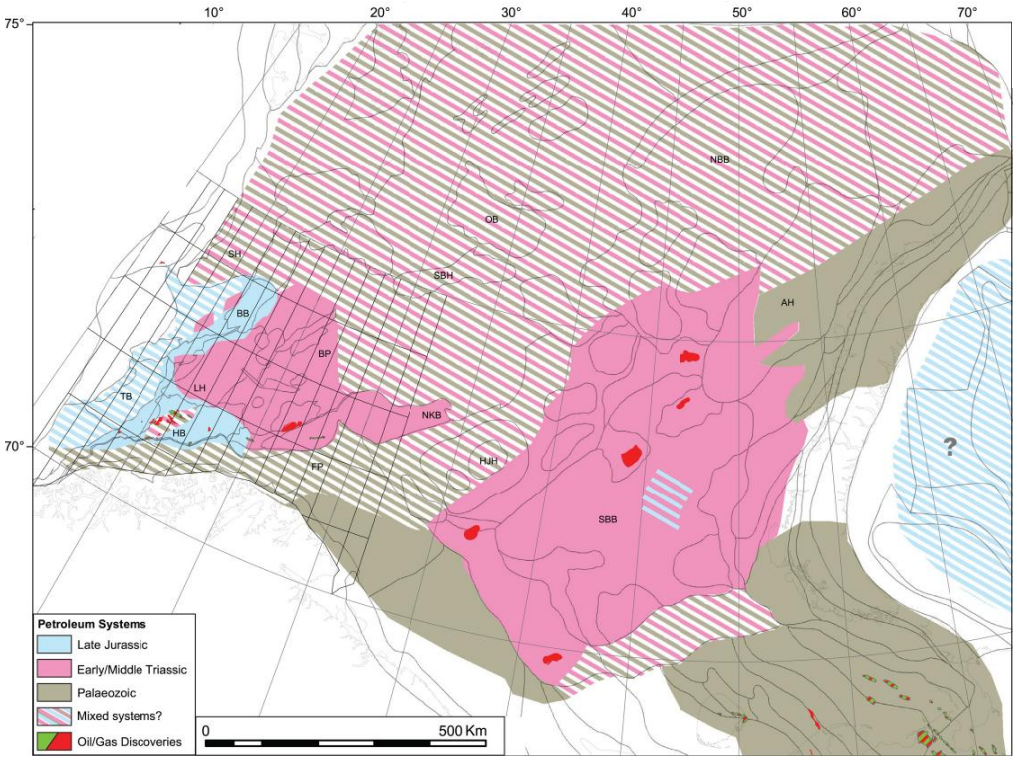

A)

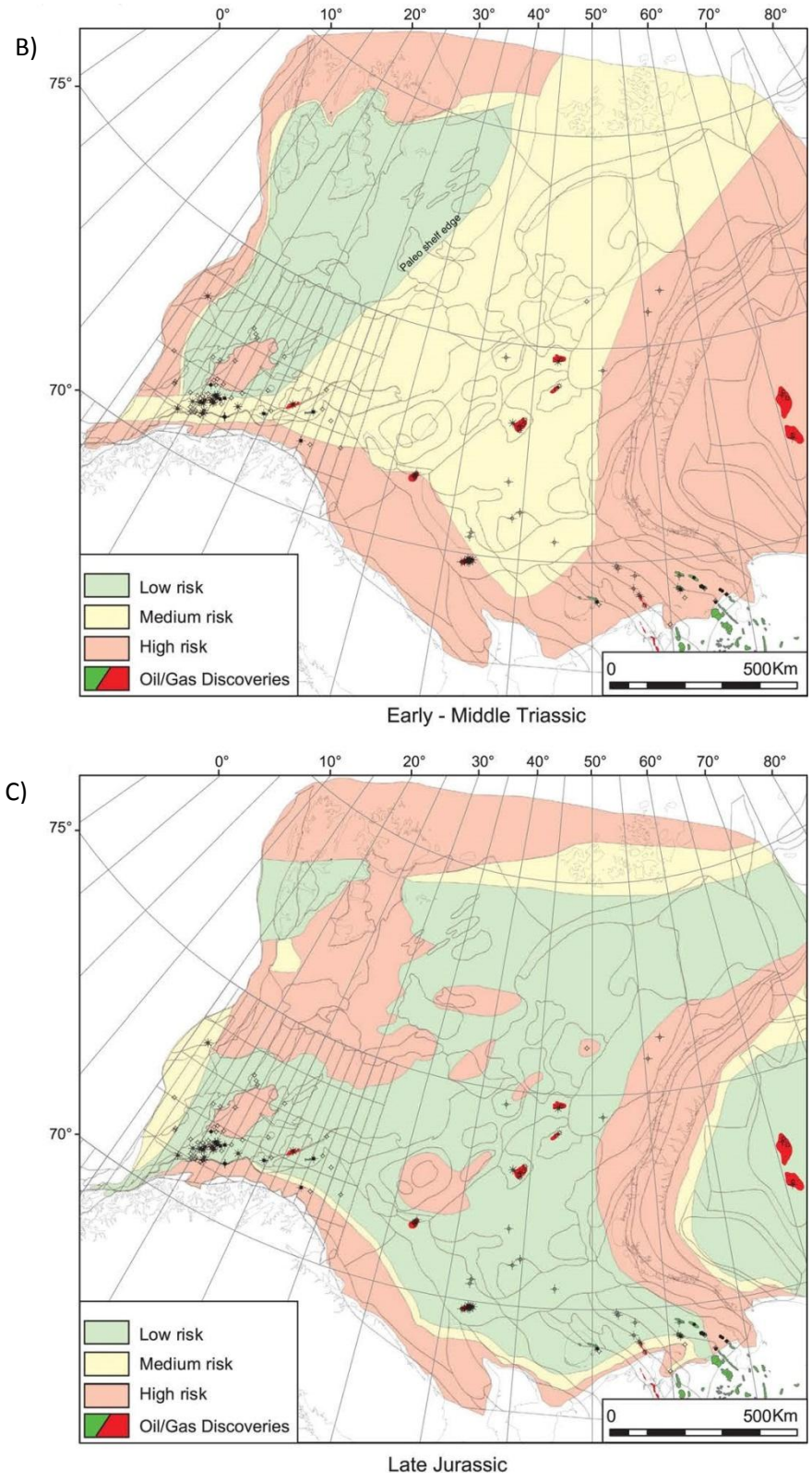

Figure 1.1 . In (A) the source rocks age is shown along all the Barents Sea; maps (B) and (C) show the risk connected to the exploration when source rocks are, respectively, Triassic and Jurassic. (From Henriksen et al 2011)

1.1 THESIS OUTLINE

Chapter 1: The aim of this first chapter is to provide a brief introduction of the topic, underlying not only the scientific relevance, but also the implications with hydrocarbon exploration.

Chapter 2: It provides a geological setting of the area including: (1) an overview of the evolution of the area, from a geological and tectonic point of view; (2) a description of the stratigraphy and of the main lithostratigraphic units; (3) a summary of the conceivable thermal histories developed in previous studies.

Chapter 3: It describes the methods and the procedures used for this work giving a definition of the basic concepts of the low temperature thermochronology and an accurate overview of the (U-Th)/He method, besides the software used for the appraisal of the data.

Chapter 4: It includes a description of the material and the procedures to prepare the samples for the analysis.

Chapter 5: It presents (1) the analytical data, displayed through tables and diagrams and subsequently described; (2) the specific modelling methods adopted for this study.

Chapter 6: It deals with discussion and interpretation of the thermochronological data.

Chapter 7: In this chapter all the knowledge and the information are related in order to summarise the whole work

CHAPTER 2
GEOLOGICAL SETTING

2.1 REGIONAL CONTEXT

The study area is located in the Barents Sea region that is part of the Norwegian offshore territory. This area has been explored since 1980 when the Sea was opened for drilling. During a first stage of exploration, attention was focused on the Tromsø and Hammerfest Basins and, just later, to the Loppa High region, situated on the south-eastern margin of the Bjørnøya Basin and the northern margin of the Hammerfest Basin (Gabrielsen et al., 1990). The Barents Sea is limited by the north Norwegian and Russian coasts, the Russian archipelago of Novaya Zemlya, Franz Josef Land and Svalbard. This defines an area of about 1.3 million km^2 with an average water depths of about 300 m (Dorè, 1995) and a maximum of ca. 2000 m when it joins the oceanic Norway and Lofoten basin where the Barents Sea separates from the Greenland and Eurasian basins (Faleide et al., 1993). These features make it one of the largest areas of continental shelf on the globe (Dorè, 1995).

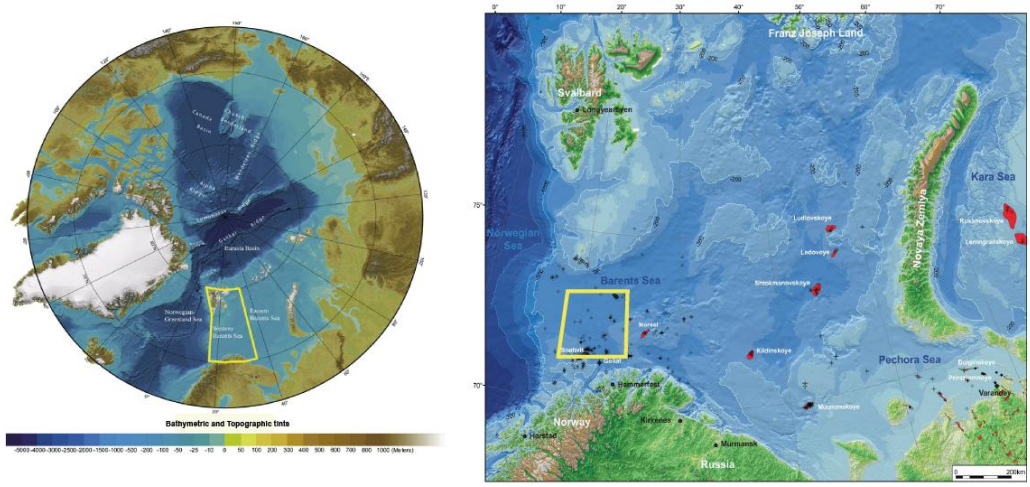

Figure 2.1 . The studied area is highlighted by the yellow squares at different scales in the two maps, where bathymetry and topography are well rendered. (From Gløstrad-Clark et al., 2010 and Henriksen et al., 2011)

The Barents Sea can be ideally divided into two parts due to structural elements: the western one and eastern one (Faleide et al., 1993). The western part, according to Faleide et al. (1993), can be further subdivided into three sections, once more due to fault zones. Briefly, this partition separates: (1) the Svalbard Platform which has acted as a stable platform since late Paleozoic times and it is covered by almost flat-lying Upper Paleozoic and Mesozoic strata; (2) the basin portion between Svalbard and Norwegian costs where are located a number of sub-basins and high; (3) the western continental margin.
The wells sampled for this work are located on the western Loppa High margin. This structural high is situated approximately between latitudes 71°80'N and 73°20'N and between 20°E and 22°E in longitude (Cavanagh et al., 2006) on the highly block-faulted area of the basin according to Faleide et al. (1993) partition. It is linked to a positive gravity and magnetic anomalies due to a relatively shallow metamorphic basement. The shallow depth of the basement is probably due to a low subsidence rate, if compared to the rest of the shelf, during the Cretaceous and Tertiary extensions (Faleide et al., 1993).

2.2 STRUCTURAL ELEMENTS

The Barents Sea is a complex mosaic of basins and platforms because it has been affected by several tectonic phases since the Ordovician, when the Caledonian orogenic movements started (Dorè, 1995). The western Barents Sea holds several Jurassic-Cretaceous fault-zones that creates the boundaries between basins and highs. In evidence: The Troms-Finnmark Fault Complex, the Ringvassøy-Loppa Fault Complex, Bjørnøyrenna Fault Complex and Leirdjupet Fault Complex that constitute the western margin of the Loppa High (Faleide et al., 1993). Barents Sea is so bracketed by some tectonic lineaments which are dominant and active on different regions and periods.

NE–SW trends

In the Barents Sea, there are two faults lineaments with a NE-SW orientation. The south-eastern portion of the shelf is characterized by a block faulting which is the offshore representation of the onshore Møre–Trøndelag fault zone. The western part of the shelf is marked by a parallel lineament called the "Lofoten Line", which shaped the area during Mesozoic and Cenozoic extension, even if its origins are probably older. This fault trend has been well studied thanks to gravity images that highlight the presence of these structures (Dorè et al., 1997).

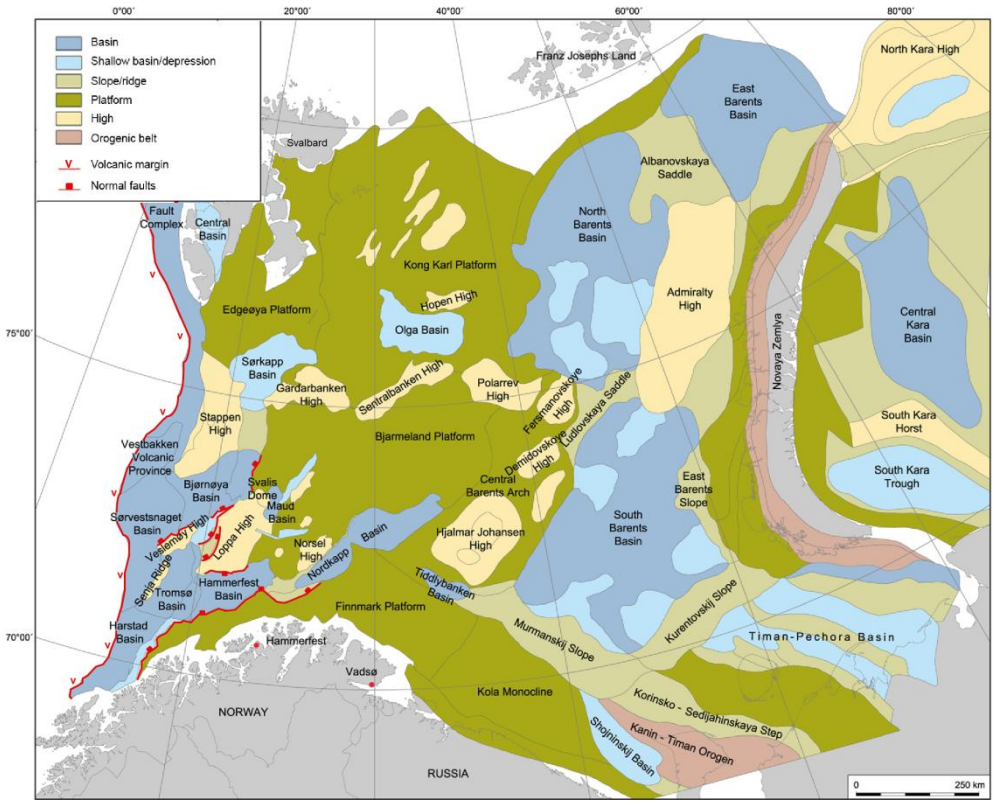

A)

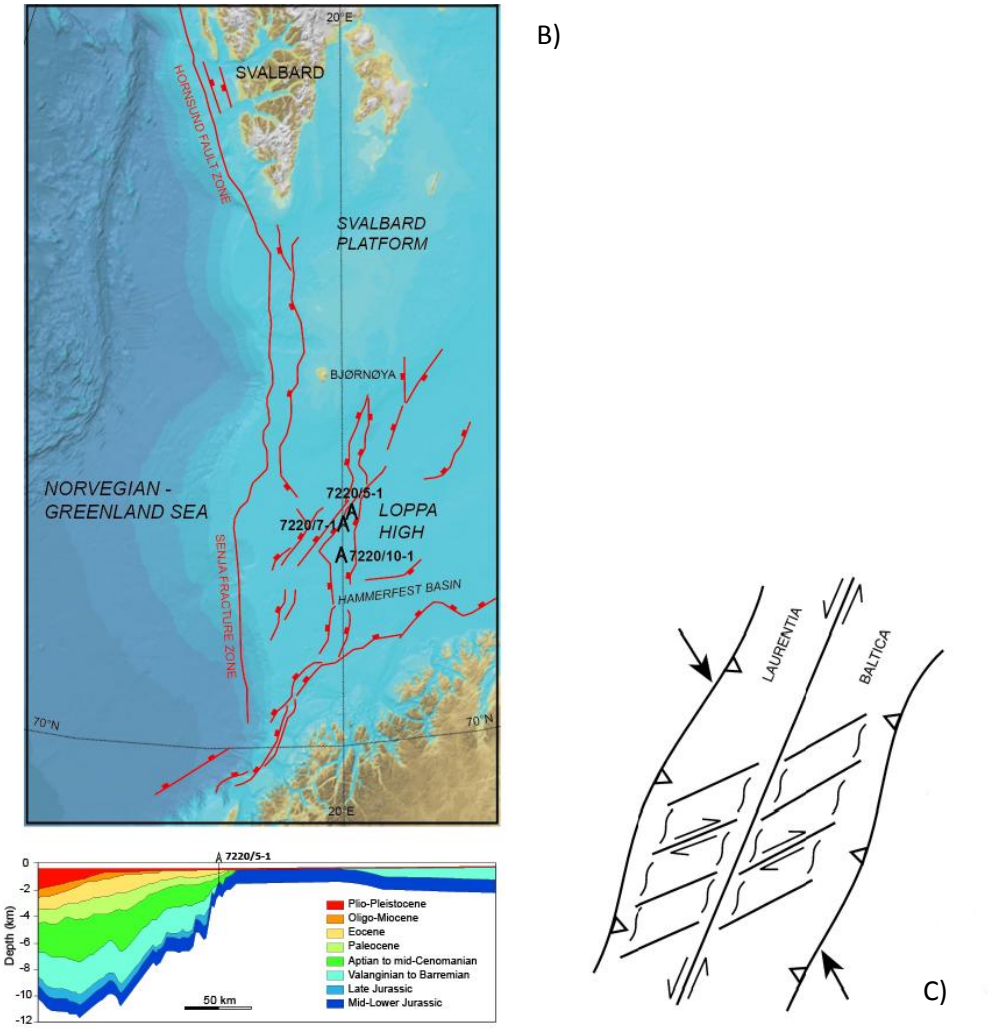

Figure 2.2 . (A) Structural asset of the Barents Sea and the main tectonic features in the range of the studied area (From Henriksen et al., 2011). (B) Magnification on the studied area and cross section through one well location; (C) Schematic suggestion of the generation of the main tectonic pattern in the area of interest (NE-SW) due to an oblique shearing during the Palaeozoic drifting (From Dorè et al., 1997).

N–S trends

In the northernmost part of the Sea, N-S lineaments are dominant (Gabrielsen et al., 1990). According to Dorè et al. (1997) the main N-S fault system is surrounded by numerous smaller faults parallel to it. Even this lineament is well understandable by exploiting gravity images that show a block faulting involving the basement. Interaction between N-S systems and NE-SW lineaments creates an overall widespread rhomboidal geometry at a variety of

scales. This evidence suggests a common origin of the two fault sets, even if this hypothesis has not to be yet proven (Dorè et al., 1997).

NW–SE trends

This transfer fault set was probably active during Mesozoic and Cenozoic times and it played a role in the Mesozoic evolution of the Greenland northward rift. Similarly to both the previous faults sets, even this one shows smaller features with the same trend and evidences of a basement separation are present (Dorè et al., 1997).

A significant segmentation is visible along the whole margin, due to the multi-phase extensional deformation. The Vøring Margin, along which the Senja Fracture Zone and the Vestbakken Volcanic Province developed, marks the western limit of the continental shelf. It is almost 500 km wide and divides the Vøring Basin from the Vøring Plateau highlighting the passage from the oceanic crust of the Norwegian-Greenland Sea to the continental shelf. The difference between the crustal thicknesses of the two parts is noticeable. It varies from 4-10 Km in the eastern oceanic portion to 30-32 Km near the coastline of the western Barents Sea. The transition is represented by the Vøring Margin that consists of an anomalously thick oceanic crust on one side and a stretched continental crust on the other, producing once more an alternation of structural highs and basins (Faleide et al., 2008).

2.3 TECTONIC EVOLUTION

This large scale block faulting took place between the Late Devonian and Early Carboniferous times (Gabrielsen et al., 1990) due to a continental separation occurred at the end of the Caledonian mountain-building episode, culminated approximately 400 Ma. It represented the closure of the Iapetus Ocean. As a result, the Laurentian and Baltic Plate merged into the unique merged Laurasian continent (Dorè, 1995).

After the Carboniferous block faulting, deposition in the new-formed basins marked the beginning of thermal subsidence (Dengo and Røssland, 1992).

Since Permian to Late Triassic, a period of an almost tectonic quiescence occurred, marked by evaporites deposition, while the eastern margin of the Barents Sea was forming by collision. This event occurred during the last stages of the Uralian orogeny that was the final element of a global occurrence which drove the world's landmasses to merge into the single supercontinent Pangea (Dorè, 1995).

During Late Mesozoic period a new crustal extension involved the Barents Sea producing a noticeable subsidence in the western basins (Dengo and Røssland, 1992) and exhumation in other portions. This second important tectonic stage in Barents Sea history was triggered by a sea floor spreading due to the opening of the Amerasian Basin in the Arctic Ocean (Dörr et al., 2012) because of the break-up of Pangea (Dorè, 1995).

A new main tectonic event occurred during the Late Paleocene due to a landmasses re-organisation (Dörr et al., 2012) because of the development of a passive margin along the western part of the Sea (Dengo and Røssland, 1992), as a response to the opening of the Nowegian-Greenland Sea (Faleide et al., 1993).

Since Neogene, contractional deformation developed along the passive margin due to basin inversion (Dengo and Røssland, 1992), related to the position along the developing Atlantic and Arctic oceans (Dorè, 1995).

The Barents Sea area drifted northwards from a paleolatitude of 20˚N during Carboniferous to 55˚N in the Triassic times, and from then on progressively to its present position of about 75˚N. Carbonate deposition (with some important evaporite intervals, as previously hinted) prevailed over wide areas of the shelf until Permian times; from the Triassic onward clastic deposition of sands and shales was dominant (Dorè, 1995).

2.3.1 CENOZOIC EVOLUTION

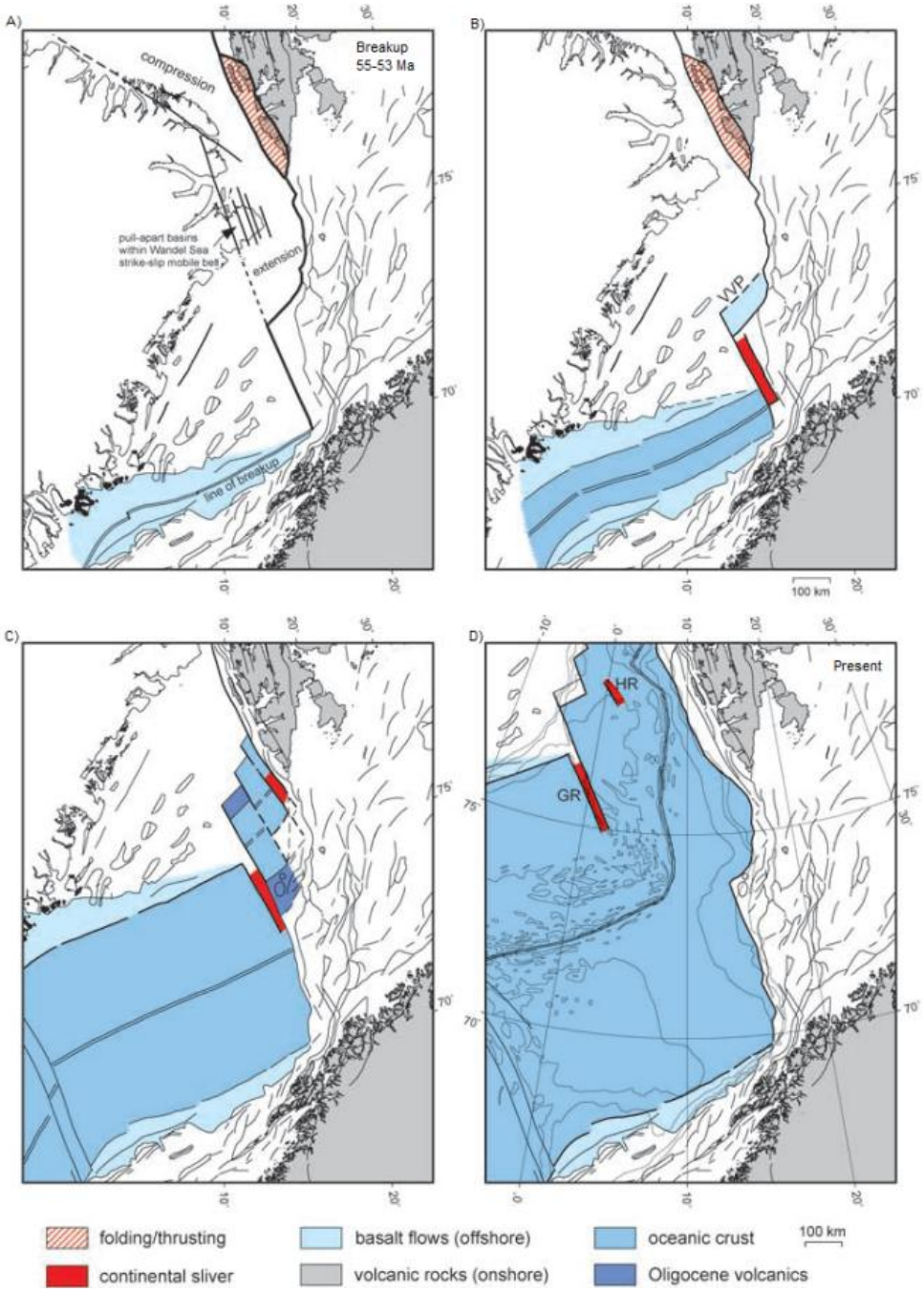

Figure 2.3 . Cenoozoic evolution of the western margin (From Faleide et al., 2008)

The last crustal extension experienced by the Barents Sea begun in the Last Cretaceous and ended up at ca. 53 Ma by re-activation of Mesozoic faults

(Faleide et al., 1993). This tectonic context produced the well-defined pull-apart basins visible today in the southwest (Faleide et al., 1993). Associated to this event, a noticeable rotation of strata and blocks occurred due to the detachments; this rotation induced localized melting (Dorè et al., 1999, Cavanagh et al., 2006) .

Later a inversion of the horizontal stress patterns took place and a NW-SE compressive regime has been activated still today (Dorè et al., 1999). It took place between 30 and 15 Ma and generated a widespread occurrence of shallow marine conditions (Cavanagh et al., 2006). This new stress pattern is consistent both with the developing of Atlantic and Arctic oceans, as previously stated, and with the relative motion of Europe and Africa. Moreover, specific observation suggests a systematic younging of the inversion moving northward (Dorè et al., 1999).

The very last tectonic phase is the regional uplift located on the Atlantic margin that shaped the today landmasses distribution and could has had critical effect of the Norwegian petroleum systems (Dorè et al., 1999). Some previous studies (Dorè et al., 1999 , Laberg et al., 2012) suggested that a third exhumation phase could have been active during Plio-Pleistocene, considering a magnification of the local uplift during the last few million years due to glaciofluvial, or full glacial, conditions. Ice sheets appeared during a early and middle Cenozoic climatic deterioration dated between 2,7 Ma (Laberg et al., 2012) and 2,5 Ma (Cavanagh et al., 2006). At that time the Barents Sea was, partially, a subaerial platform and a strong glacial erosion caused an isostatic uplift during the inter-glacial periods (Dorè et al., 1999). Timing of glacial activity was driven by Milankovitch periodicity that gave ice covers through cycles of ca. 100.000 years (Cavanagh et al., 2006).

2.4 STRATIGRAPHY

Seismic data allow the observation of sedimentary sequences, not particularly deformed, for noticeable extents. The greatest difficulties are recognisable in the south-western part of the Sea because of a strong isolation of strata due to structural gaps between basins and highs (Faleide et al., 1993). Anyway Mesozoic sequences have been well correlated thanks to the drilling information in the Tromsø and Hammerfast Basins and Loppa High areas (Faleide et al., 1993).

Triassic deposits played a key role in the Barents Sea history because shallow marine and continental sandstones are identified as important reservoir rocks in all formations (Gløstrad-Clark et al., 2011). All over the Sea, thick Triassic rocks show transgressive-regressive depositional cycles, highlighted by coarsening upward sequences (Faleide et al., 1993) and well-rendered in 2D seismic data (Gløstrad-Clark et al., 2011). The evidence of these cyclic stages have been well preserved because sedimentation took place in a wide and relatively shallow epicontinental basin where slight sea-level variations could move the shoreline for several hundred kilometres (Gløstrad-Clark et al., 2011). Sandstones are clearly dominant from the Triassic in the southwestern area of the Barents Sea (Faleide et al., 1993). This change was probably due to a progressive transition from arid to humid climate (Gløstrad-Clark et al., 2011), that could be traced back to the Carnian Pluvial Event thanks to palynological assemblage data (Hachuli and Vigran, 2010). As a result, run-off increased together with the erosion and transport of clastic sediments from the lands to the seas. These sediments are recognisable in the basins around Loppa High and the Finnemark Platform and on the highs themselves, where the strata were later partially eroded (Faleide et al., 1993). Indeed, during Early Cretaceous, part of the Loppa High emerged and clastic fans developed in the Hamerfest Basin direction, while thinner sediments were deposited in the deeper part of the basins (Faleide et al., 1993). The progressive rifting produced deep basins, particularly in south-eastern Barents Sea, where, during

the Jurassic time, organic-rich shales were deposited, representing another very important group of source rocks of the area (Gløstrad-Clark et al., 2011). Source rocks are interpreted to be on the offlap break along clinoform geometries (Gløstrad-Clark et al., 2010). The good quality of Mesozoic source rocks could be linked to the fact that, both in Triassic and Jurassic periods, anoxic bottom conditions could have prevailed in the basins. The paleo-Loppa High has been suggested, according to Gløstrad-Clark et al. (2010) as an example where modified and limited circulation of water probably produced the accumulation of organic matter.

Geochemical analysis were performed on oil samples from the Loppa High, where the wells involved for this work are situated. Results of the pristine/phytane ratio and $\delta^{13}C$ isotopes analysis identified typical characteristics of Triassic hydrocarbons. Type II kerogene due to origin in anoxic marine condition was detected. The main marine source rocks are effectively Triassic or Jurassic all over the Barents Sea. These rocks give products with excellent qualities such as a TOC (Total Organic Carbon) percentage ranging from 1% to 12% and Hydrogen Index from 60 to 600 mg HC/g TOC. On the Norwegian shelf, there are different depositional environments. On the northernmost part of the Sea, in Svalbard area, organic-rich shales formed in highly anoxic conditions are predominant, but, moving to the south, shallow marine anoxic siliciclastic strata become prevalent. Maturity, generation and expulsion strongly change due to the local tectonic assets; anyway, most of the source rocks are oil-prone. Some gas is provided by the eldest Triassic source rocks (Bjoroy et al., 2010).

The studied samples, that will be described in chapter four, come from two different wells located on the Loppa High. One is the ENI Norge exploration well 7220/10-1 (Salina). Its exact geographical coordinates are: N 72°00’57.351” E 20°03’25.152” and it is set 382 m below the main sea level. Salina presented two proved reservoirs bearing gas. The top of first one is at -1291 m and it lasts for 134 m in sandstones and siltstones till the gas-water contact. The second reservoir is located within the Stø Formation’s good

quality sandstones between -1513 m and -1567 m (Final well report: 7220/10-1, 2012). The second well is Havis, the Statoil exploration well 7220/7-1. Its location at seabed is defined by the following geographical coordinates: N 72°27'37.5" E 20°09'08.6" , set 405 m below the main sea level. Havis is located within the Bjørnøyrenna Fault Complex; the hydrocarbon trap is structural and its seal was considered the main risk. The probability of success was estimated 58% during the pre-drill phase. The main result of the well exploration is the discovery of a 175 m thick column of hydrocarbons, both oil and gas, situated in Early-Middle Jurassic strata. The top of the reservoir is within the Stø Formation at a depth of 1741 m, the gas-oil contact has been found at 1789 m followed by the oil-water contact at -1916 m (Havis discovery evaluation report, 2012). Both well 7220/10-1 and well 7220/7-1 show a thick Cenozoic clay cover. The material was so collected from the underlying Mesozoic sediments, from Cretaceous to Upper Triassic strata. The following logs show a synthetic stratigraphy of the two exploration wells and where the samples were collected.

As shown in the logs in figure 2.4, samples were collected from the Kapp Toscana Group, specifically from the Realgrunnen Subgroup. It is divided into Fruholmen, Tubåen, Nordmela and Stø Formations and its thickness can intensely change even of hundreds metres. The lower boundary corresponds to the basal shale of the Fruholmen Formation (Norian). Deposition took place mainly in near-shore deltaic environments, characterized by shallow marine and coastal reworking of deltaic and fluviodeltaic deposits. A description of the Formations is discussed below (www.npd.no).

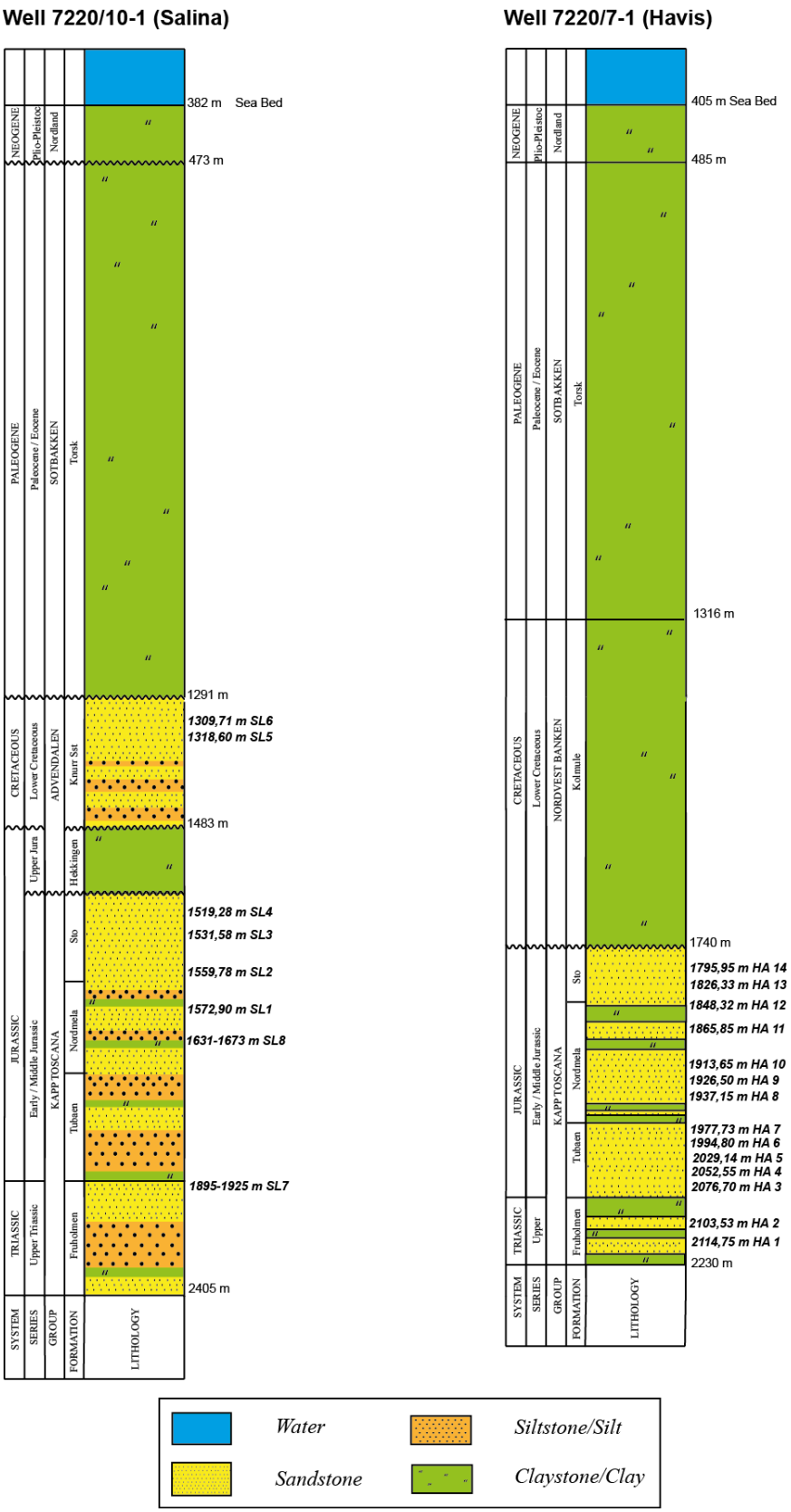

Figure 2.4 . Schematic logs of the wells sampled for this work.

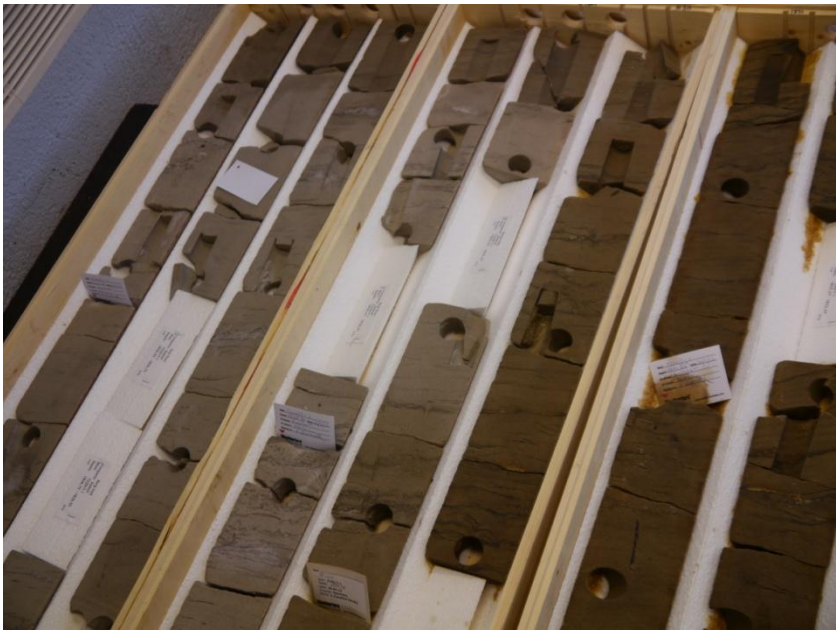

Figure 2.5 . Overview of some of the sampled cores at the depth interval of reservoir rocks.

2.4.1 SAMPLED FORMATIONS

The *Fruholmen Formation*

This Formation covers a period from Norian to Rhaetian. The lithological development allows a subdivision within three parts. The first, the lowermost part of the Formation, shows the remarkable presence of grey to dark shales (Akkar member). The second part is the Rake Member, which overlay the first, and is characterised by the dominant presence of sandstones. The third part is the shale-rich Krabbe Member. The sedimentologycal interpretation is a prograding fluviodeltaic depositional environment which presented many stages of lateral shifting.

The *Tubåen Formation*

The Formation is Rhaetian to Hettangian. Even here a theoretical treble subdivision have been performed: the sand-rich lower and the upper parts are separated by a middle portion where silt and shale are more abundant. The sandstone of the Tubåen Formation are thought to be fluvial and delta deposits such as tidal inlet or estuarine environments.

The *Nordmela Formation*

It is Sinemurian to Late Pliensbachian. Decreasing from the bottom to the top, there are interbedded siltstones, shale and mudstones with minor coals; on the contrary, sandstone layers increase toward the upper part of the Formation. The coarser sediments represent estuarine and tidal channels, while the thinner parts are representative of tidal flat or flood plain.

The *Stø Formation*

It is Late Pliensbachian to Bajocian. The Stø Formation main lithology is given by mineralogically mature and well sorted sandstone although some conglomerate can be found along the section. The Formation was deposited in a prograding costal regime and it can be subdivided by three transgressive episodes. (www.npd.no)

2.5 THERMAL HISTORIES OF BARENTS SEA: PREVIOUS STUDIES

Hydrocarbon generation is temperature dependent so it is crucial to include thermal history to make the basin modelling significant. Therefore, a first essential input to predict gas and oil generation is the heat flow history.

The heat flow is a function of: basal heat flux, thermal conductivity of rocks and the surface temperature (Cavanagh et al., 2006). Typically, on the continental lithosphere this parameter varies between 40 and 90 mW/m^2. The south-western area is an intra-cratonic field and, at present, heat flow has to be considered in a range of 60-70 mW/m^2, that corresponds to a geothermal gradient of about 30°C/km (Green and Duddy, 2010). Moreover previously tested models affirm that in the past, since Late Palaeozoic, this value was slightly lower than today (Cavanagh et al., 2006) or it even didn't changed (Green and Duddy, 2010).

Different simulations were performed to understand the timing of the uplift in the studied area. Measured data from AFT analysis (apatite fission

tracks analysis) and VR (vitrinite reflectance) were used (Cavanagh et al., 2006). The first simulation performed by the authors clearly favoured an exhumation linked to a very recent glacial erosion. The outcomes, indeed, imply a very recent uplift produced by an isostatic rebound due to sediment removal. Nevertheless some problems affected this model. Errors may be introduced by an unrealistic heat flow history for the Cenozoic period and the developing of contradictions with both local evidence of compressional deformation and with the widely accepted maturity peak reached during the Oligocene-Miocene. Therefore a second simulation was performed by using the Carr & Scotchman (2003) method, that strongly links the heat flow variation to the burial history. Inaccuracies were so avoided by performing this second try. Results reveal to be well related to the Oligocene-Miocene maturity peak and they didn't shown any contradiction with other evidences. This second simulation well described an exhumation that started 30-15 million years ago, not excluding a further Pleistocenic uplift; however the model results to be unaffected by this very last event.

A further model stage was performed by merging the Carr & Scotchman method's results and a calibrated simulation of the Plio-Pleistocenic glaciation scenario. The cyclical nature of the phenomenon, temperatures, thickness of ice sheets and the effects on the subsurface were so considered as relevant parameters. Finally an exhumation event condensed in less than 1 million year has been carried out as a main result. Simulation, thus, showed a progressive and extremely recent cooling of rocks, overlaid by periodic exhumation related to cyclic presence of ice load and erosion. Evaluation of the erosional activity of ice sheets should be increased for structural highs if compared to the basins' one. Besides this third stage of modelling keeps the Oligo-Miocenic maturity peak true.

Further models were performed by Green and Duddy (2010) by using AFT analysis and VR data. Considering an almost constant heat flow, a thermal history constrained basically by exhumation is implied. Results highlighted two dominant cooling episodes: (1) one between 40 and 20 Ma; (2)

and a second one in a more recent time, from 15 Ma to present. Anyway no significant cooling are linked to glacial activity in the latest million years. This does not exclude a remarkable uplift and erosion during recent times, but these amounts are negligible if compared to earlier events. Analogue results were obtained by studying other circumpolar areas such as northern Alaska, Arctic regions and Greenland. Furthermore, thermochronological data revealed a synchronous exhumation in these Arctic regions. Data from all the sampled territories show consistent results for a significant cooling both around the Eocene times, and during a previous episode in the Late Paleocene (60-55 Ma). Both the episodes are probably due to widely extended regional tectonic events. In contrast the Plio-Pleistocenic exhumation seems not to reach a similar consistency degree as the previous episodes, anyway uncertainties are still present and further studies were suggested.

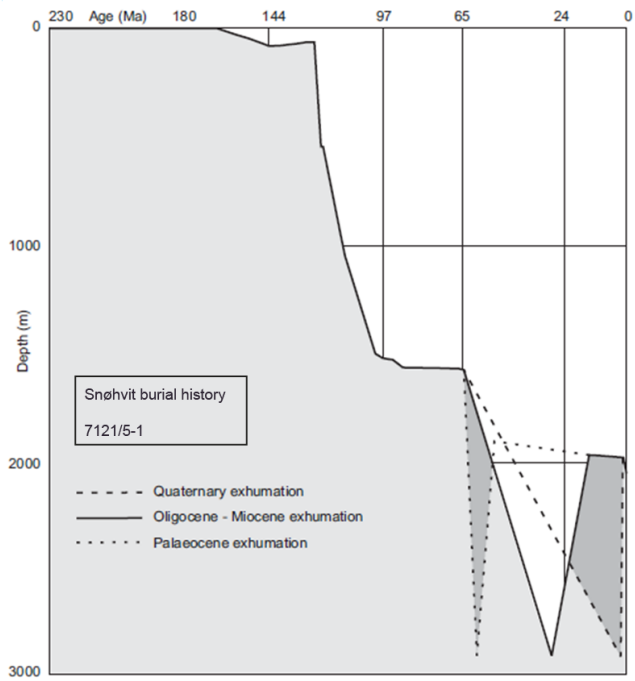

Figure 2.6 . Burial history for well 7121/5-1. All exhumation scenarios are shown for comparison (From Cavanagh et al., 2006).

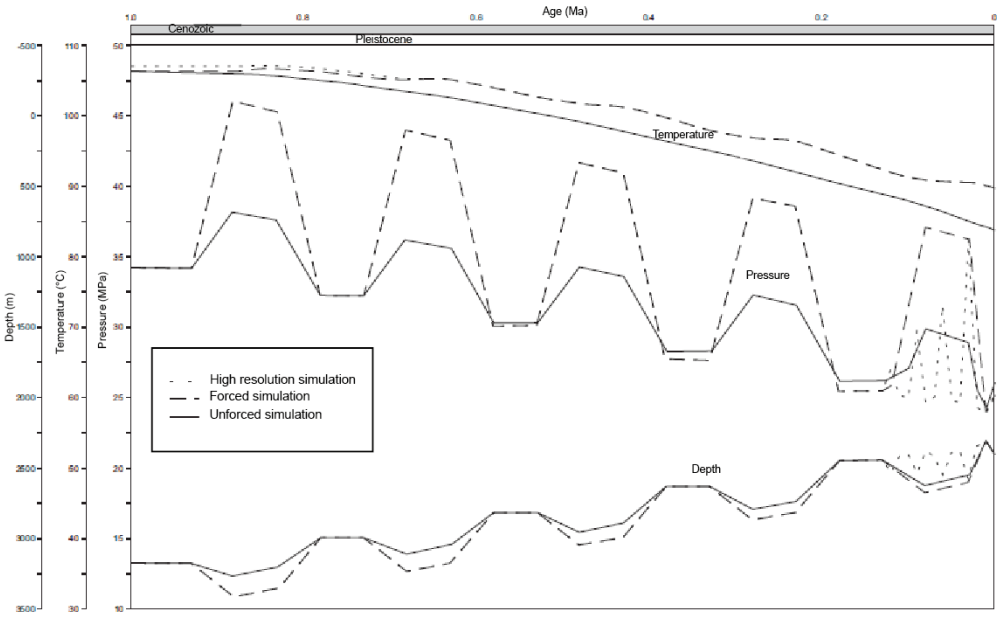

Figure 2.7 . In the graphic the fluctuations of temperature, pressure and depth are represented over a time period 1-0 Ma, according to the third stage of modelling from Cavanagh et al., 2006.

CHAPTER 3
METHODS

The following section describes thermochronological methods applied on the samples during this work. In particular, the theoretical bases of U-Th/He technique will be illustrated.

3.1 THERMOCHRONOLOGY

Thermochronology can be defined as the quantitative study that allows the reconstruction of the thermal histories of rocks using temperature-sensitive radiometric dating methods. These methods are based on the comparison between the observed abundance of a naturally occurring radioactive isotope and its decay products. The dating is achieved through well-known decay rates equations, that varies for different isotopes, and the calibration on a vertical succession of strata previously recognised from a geological point of view.
The term "thermochronometer" defines a radioisotopic system consisting of radioactive parent, radiogenic daughter or crystallographic feature, and the mineral in which they are found (Reiners et al. 2005). The thermal sensitivity of radioactive systems depends on their tendency to turn from a closed to an open system condition with increasing temperatures and viceversa, also known as the moment when diffusion starts, or stops, to obliterate the daughter product content.

In order to produce an efficient interpretation it should be given the specific meaning of some technical words and expressions listed as follows. First of all the closure temperature (Tc) can be defined as the temperature of a system at the time given by its apparent age due to the turning into a closed system. This phenomena occurs through a range of decreasing temperatures for which the retention of products of the decay by the system progressively increase from 0% at the base (maximum temperature) to 100% at the top (minimum temperature): this temperature interval is defined Partial Retention

Zone (PRZ) (Andreucci, 2013). The term reset is used to refer to minerals which experimented at least once a re-opening of the system before the final cooling to the surface temperature.

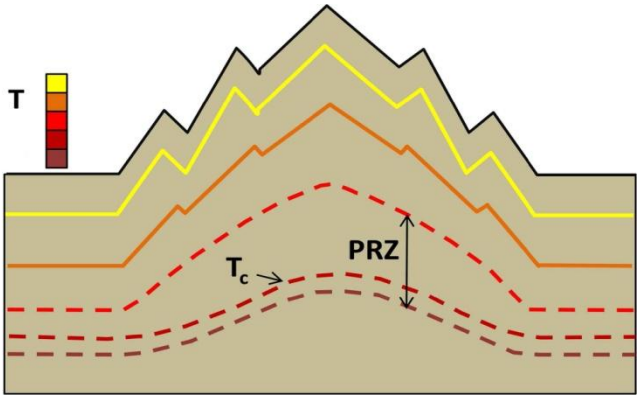

Figure 3.1 . Schematic representation of PRZ and Tc concept. The coloured lines indicates isotherms. (From Andreucci, 2013)

Therefore thermochronology measures the timing and rates at which rocks cool and approach the surface so it could be use to produce descriptions of exhumation and burial history of rocks meant as vertical motion due to tectonic or to a sediment removal or supply (not to be excluded a combination of the two).

To investigate the vertical motion of rock masses within the upper part of the Earth's crust, between 1 and 3 km, apatite fission track (AFT) and apatite (U–Th)/He (AHe) are commonly used. Isotope decay system (U-Th)/He analysis and fission tracks examination can be performed both on zircon and apatite crystals. These thermochronometers are characterised by different closure temperatures and sensitivities but all of these belong to the lower temperature thermochronology.

In this work only (U-Th)/He analysis were considered and it has been performed just on apatites in order to cover the coolest temperature ranges.

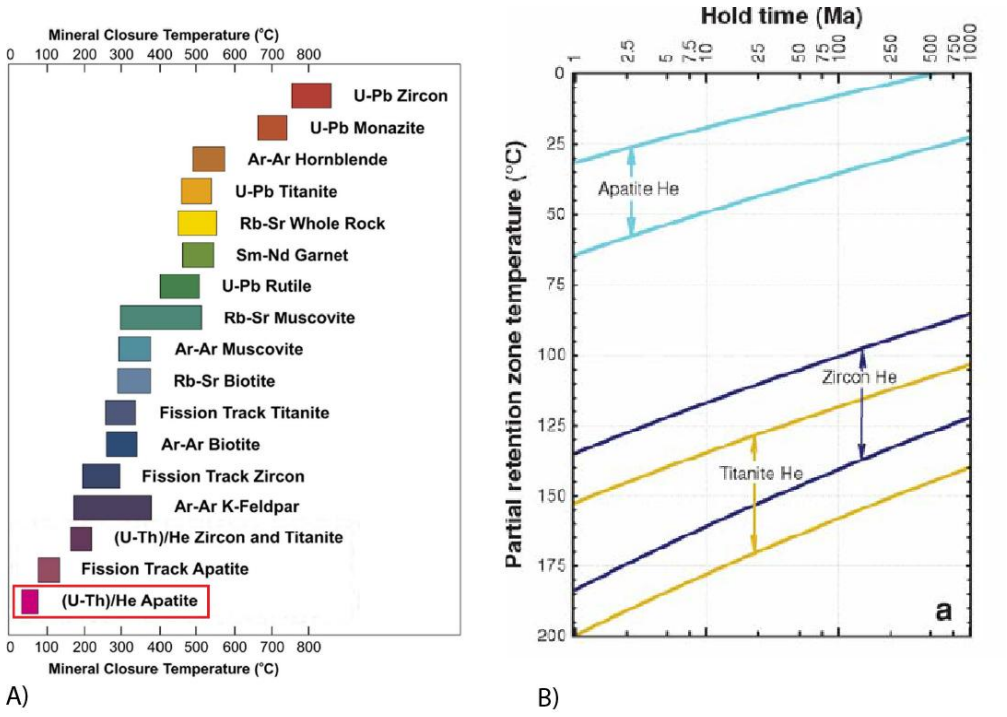

Figure 3.2 . (A) Nominal closure temperatures of various geochronometers and thermochronometers. Systems are ordered by closure temperature on the Y-axis; the red square highlights the thermochronometer used in this work. (B) Partial Retention Zones for He as a function of hold time. The upper and lower boundaries indicate respectively 90% and 10% retention. (From Reiners and Brandon, 2006)

Apatite is a common accessory mineral in igneous and metamorphic rocks and it could be easily recognised in clastic sedimentary rocks due to its high preservation potential. The term "apatite" identifies a group of isomorphous hexagonal phosphate minerals, following the chemical formula Ca_5 [(F,Cl,OH) $(PO_4)_3$]. The focus on apatite arises from its ubiquity and moderately high U and Th content, but more importantly because He accumulation in apatite occurs only at temperatures below 70-75°C; at higher temperatures diffusion removes He as fast as it is produced by decay (Reiners and Brandon, 2006).

3.2 (U-Th)/He METHOD

The (U-Th)/He method (He dating) is based on the accumulation of ^{4}He produced by the decay of the parent isotopes ^{238}U, ^{235}U, ^{232}Th, and ^{147}Sm through α-emission. The ingrowth equation gives a quantitative indication of the amount of He that could be accumulated by decay:

$He = 8\ ^{238}U\ (e^{\lambda_{238}t} - 1) + 7\ (^{238}U/137.88) \cdot (e^{\lambda_{238}t} - 1) + 6\ ^{232}Th\ (e^{\lambda_{238}t} - 1)$

Where λ is the decay constant and it takes the following values depending on the isotope: $\lambda_{238} = 1.551 \times 10^{-10}\ yr^{-1}$, $\lambda_{235} = 9.849 \times 10^{-10}\ yr^{-1}$, $\lambda_{232} = 4.948 \times 10^{-11}\ yr^{-1}$. Anyway some assumption have to be considered. The truthfulness of the equation is guaranteed only when the initial amount of ^{4}He is null and for crystals formed at least 350 000 years ago. The first assumption is, in general, a good hypothesis because He has a very low concentration in atmosphere (5 ppm contrary to ~1% for ^{40}Ar, highly used for dating) that trapped atmospheric He is unlikely to be important. Anyway it could possibly occur (Farley, 2002). Diffusion rate of radiogenic ^{4}He out of the mineral is determined by the temperature and the He diffusivity of the mineral. While in the case of rapidly cooled rocks at the Earth's surface, volcanic for example, retention at ~25ºC is sufficient to successfully apply He dating, thermochronometry of slowly cooled rocks requires precise knowledge of how diffusivity scales with temperature (Farley, 2002). Moreover, the Tc of mineral grains is dependent on a geometry factor for the crystal shape, the length of the average diffusion pathway from the interior to the surface of the grain and the cooling rate (Reiners and Brandon, 2006). Usually PRZ for AHe between 40°C-80°C (Farley, 2002). Specifically for cooling rates of 10°C/Ma and diameter of the spherical domain of 60 μm, AHe Tc could be estimated ca. 67°C (Reiners and Brandon, 2006). Between the PRZ limits, He ages are very sensitive to temperature, with variations of millions of years possible over very small depth increments. While in PRZ temperature range, He ages will increase with calendar time because ingrowth exceeds diffusive loss, but the age increase will be less than the increase in calendar time (Farley, 2002).

Once acquired this basic information the concentrations of ^{4}He and of the parent isotopes and a cooling age can be deducted. Measurements are typically made using a two-stage analytical procedure involving degassing of the crystal under vacuum by heating with a Nd-YAG laser and gas-source mass spectrometry to measure $^{4}He/^{3}He$ ratio. U, Th and Sm concentrations are finally obtained by isotope dilution using an inductively coupled plasma mass spectrometer. Grain ages typically have a relative standard error (RSE) of approximately 3% to 5%, as determined by replicate measurements (Reiners and Brandon, 2006).

Main assumptions are: the absence of ^{4}He, both initial, as stated above, and produced by sources extraneous to the crystal (for apatite the presence of external sources of He can be represented by U-Th rich inclusions, as zircons and monazite, or coating made of oxides and hydroxide); an equilibrium among all daughter products in the decay chain and a constant decay of the parents isotopes through time. In addition, ^{4}He diffusion could be impeded by damages in the apatite structure. A careful selection of the crystal is therefore required, to avoid grains affected by pervasive inclusions or broad coating.

Main data produced by these procedures of analysis are:

- → Raw age (±σ): measured age of the grain before the correction.
- → Radius: radius of a hypothetical sphere that should approximate the crystal. It is calculated as the mean between the two dimensions measured in each single grain.
- → U, Th, Sm (ppm): U, Th and Sm contents.
- → ^{4}He (nmol/g): concentration of He measured by the mass spectrometer.
- → eU (ppm): Effective Uranium, quantity typically used to represent the concentration of U and Th. It is calculated according to the formula: $eU=[U]+0.235\times[Th]$. eU<5 ppm is considered anomalous and reported in italics.
- → FT ^{238}U, ^{235}U, ^{232}Th, ^{147}Sm: is the α-ejection correction factor. The resulting dates require a correction for He loss occurred by ejection of α particles outside the crystal domain.

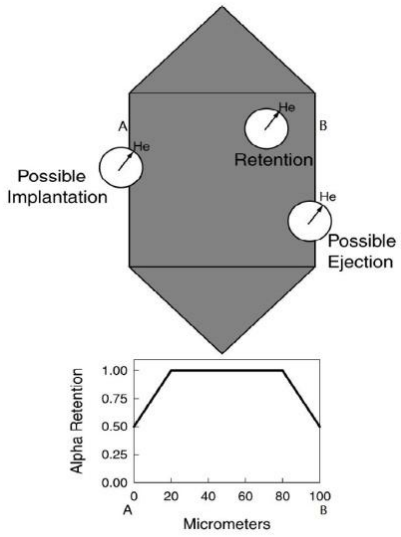

Figure 3.3 . The effects of long α–stopping distances on He retention (From Farley, 2002) . The upper figure illustrates the three possibilities within a schematic crystal: α retention, possible α ejection, and possible α implantation. The centre of the circle denotes the site of the parent U or Th nuclide, and the edge of the white circle labelled He indicates the locus of points where the α particle may come to rest; the arrow indicates one possible trajectory. The lower plot shows schematically how α retention changes from rim to core to rim along the path A-B.

When a parent isotope decays an α particles is emitted because of the kinetic energy of the reaction. In apatites the α particles travel a distance of ca. 20 μm; those emitted close to the crystal edges are ejected out of the crystal and lost. The loss of α particles leads to an underestimation of the age of the crystal. The magnitude of α-ejection is controlled by surface to volume ratio and by spatial distribution of the parent atoms relative to the crystal surface. Assuming an idealized geometry of the crystal and an homogeneous distribution of U, Th and Sm in the crystal, the fraction of He retained can be calculated as a function of the crystal size (Farley, 2002). Therefore, to account for α-ejection it is a common practice to measure the physical dimensions of the crystal to be dated and to calculate a homogeneous α-ejection correction factor, to which the raw date has to be multiplied, to obtain the corrected age (Farley, 2002).

→ Fully corrected FT age (±σ): age of the grain after the correction.

In optimal situations, 3 to 5 crystals are analyzed for each rock sample. When age reproducibility is checked, that is to say that the corrected ages obtained by the analysis converge, the mean of the ages can be used for interpretation. However, age dispersion may be present. Problems may occur in the evaluation of the sample age because it is influenced by the rightfulness of the measurements. Considering the correction values it is common to detect values of 0.75-0.90; however, this quantity can increase or decrease significantly with changes in grain size or poor grain geometry. Even a partial resetting of the samples, can lead to strong age differences among the same sample crystals. This problem is exaggerated by abrasion and rounding of the grains. Furthermore, inclusions and coating can also be misleading, since they constitute external sources of He. Finally, errors may arise in fractured or broken crystals due to an *in itinere* modification of the diffusion kinetics.
When measures are completed, a quantitative evaluation of the thermal history can be carried out through modelling procedures, which find a range of cooling paths compatible with thermochronology data.

3.3 MODELLING

To reconstruct more complex thermal histories, thermal modelling is used. Thermal modelling allows to trace the envelope of the thermal histories that best fit the measured data. The software used in this work for thermal modelling is HeFTy (Ketcham, 2005). The system allows to construct both a forward model and an inverse model based on one or more crystals data. The methods are discussed as follows.

The first step is to provide the program with the measured data. Samples are studied one by one, that is that each model will derive from the apatites of a single sample. Input data for each crystal are: (1) the radius of a hypothetical sphere that should approximate the crystal; (2) the raw age and its error margin ($\pm\sigma$); (3) the U, Th and Sm content, expressed in ppm.

Furthermore the present day temperature and the deposition temperature have to be provided. After this first step, the software will be able to calculate and the α ejection factor and thus the corrected age. At this point a forward model can be performed, in this case the user will manually define the thermal path. In the case of inverse model the user will input also time-temperature constraints if known. The program will eventually calculate the best paths that fit all the dataset. The gauge of the match between the thermal model and the measured data is given by the Goodness Of Fit (GOF). This parameter ranges between 0 and 1: it is considered "acceptable" when the value is over 0.05 and "good" when over 0.5 (Ketcham, 2013).

CHAPTER 4
SAMPLES AND PROCEDURES

4.1 MATERIALS

The collection of the materials for thermochronological analyses occurred during a core sampling at Weatherford laboratories in Stavanger (Norway) in July 2014.

A set of 20 siliciclastic sandstones samples was taken from two well's core: well 7220/10-1 (Salina) and well 7220/7-1 (Havis), whose descriptions have been discussed in the previous chapter. Each of the sample was consisting of less than 100 cc of material, thus making the finding of suitable minerals challenging. In addition, 13 cuttings, covering two different intervals, were collected from Salina well. The following table summarize the main information about all the collected samples.

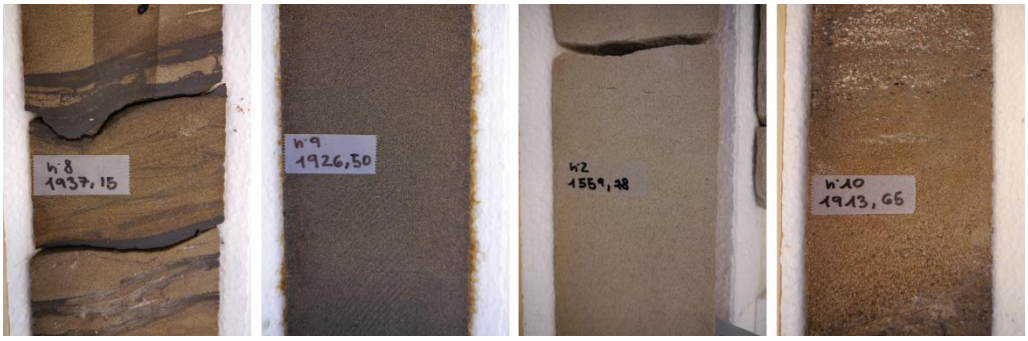

Figure 4.1 . In the photos some of the cores selected for the sample taking. Different grain size and structures are visible for comparison.

WELL 7220/10-1 (SALINA)		
Sample		***Depth***
SL1		1572,90
SL2		1559,78
SL3		1531,58
SL4		1519,26
SL5		1318,60
SL6		1309,71
Cuttings		
SL7	Cu 1	1925
	Cu 2	1919
	Cu 3	1913
	Cu 4	1907
	Cu 5	1901
	Cu 6	1895
SL8	Cu 7	1679
	Cu 8	1673
	Cu 9	1667
	Cu 10	1646
	Cu 11	1640
	Cu 12	1637
	Cu 13	1631

WELL 7220/7-1 (HAVIS)	
Sample	***Depth***
HA1	2114,75
HA2	2103,52
HA3	2076,70
HA4	2052,55
HA5	2029,14
HA6	1994,80
HA7	1977,73
HA8	1937,15
HA9	1926,50
HA10	1913,65
HA11	1865,85
HA12	1848,32
HA13	1826,33
HA14	1795,95

Figure 4.2 . The table summarizes the collected samples. All of them were siliciclastic sandstones. As concerns the cuttings, because of each cutting bag was filled with a very low quantity of material, they were gathered into two cumulative samples depending on the depth.

4.2 SAMPLES PROCESSING

All the processing procedures have been carried out at University of Padua, in the Department of Geosciences laboratories.

Both the core-chips and the cuttings were manually crushed with an agate mortar and pestle. Accurate cleaning procedures were applied in order to avoid

the contamination of the samples. Some of the crumbled material was sieved through 250μm sieve-cloth achieving a uniform sand-like particle size. The coarser fraction was reworked until it reached the correct dimensions or eliminated when unsuitable.

After grinding, samples were washed with solvent an adequate number of times in order to completely eliminate the organic matter content to avoid flocculation that could introduce mistakes during the following procedure's steps. In this work, acetone was used (chemical formula: CH_3COCH_3) as solvent at room temperature. Acetone was then removed by using distilled water and the coarse portion was separated by exploiting the slower decantation of the mud component. The thinner fraction was leaved in beckers to decant, whereas the coarser fraction was accurately re-washed with distilled water and then stored in ceramic cups put in a kiln at ca. 40°-50°C to dry the samples. Magnetic separation with Frantz Isodynamic magnetic separator was not operated for this work because both of the absence of magnetic minerals in most of the samples and because of the very small amount of material. The dried fraction was then submitted to heavy liquid separation with Sodium Polytungstate (density shown in figure 4.3).

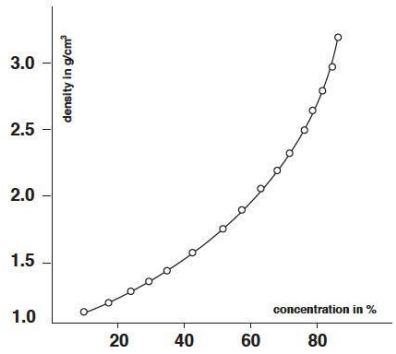

Figure 4.3 . In the graphic the density of aqueous Sodium Polytungstate solution as a function of mass portion at 25°C.

Each sample runs a spin cycle in a laboratory centrifuge allowing the deposition, on the bottom of the centrifuge's tubes, of the heavy minerals with a density higher than ρ=2.89 g/cm^3, that is both apatite (ρ=3.1-3.35 g/cm^3) and zircon (ρ= 4-4.70 g/cm^3). The solution of Sodium Polytungstate was separated

from the treated samples by using a filtering paper and further washing with distilled water. Two samples, SL3 and HA10, needed an additional separation by using glycerine (chemical formula: $C_3H_8O_3$) because of a very high concentration of pyrite in the heavy fraction with apatites. This procedure was carried out manually in beckers by decantation making pyrite-rich portion separate due to the higher density (ρ=5,1 g/cm^3).

After all the separation processes, apatites were selected by manual picking under optical stereoscope. The selection parameters for grains were previously described in the (U-Th)/He thermochronology section. Each apatite was photographed and measured and all data about crystals, even description of grains imperfections, were reported in tables for the geometrical reconstruction required for α-ejection correction. The prism length and width measurements were taken respectively parallel on the c-axis, and perpendicular to it on two orthogonal directions. Crystals were packed in Nb tubes of 1mm heights that worked as a micro-furnace for crystal heating and He extraction during analysis and then sent to the Geosciences department of the University of Arizona (Tucson).

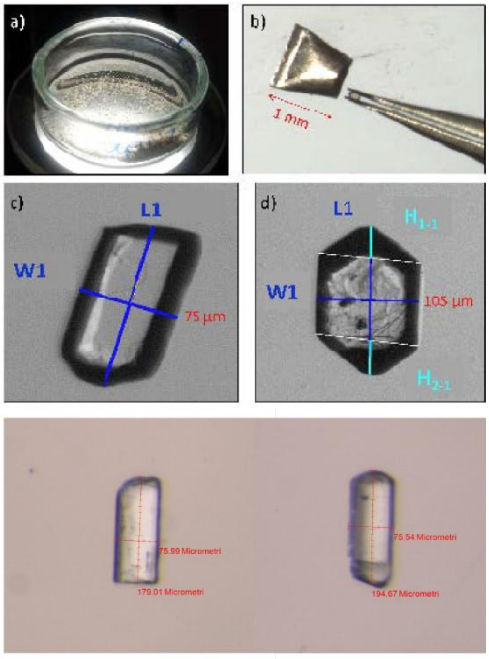

Figure 4.4 . Grain selection and picking: (a) the grains are poured in a petri-dish for grain

selection under optical microscope; (c, d) the selected grains are photographed and measured, for apatite length (L) and width (W) are measured on two sides parallel to the c-axis. (b) Grains are finally packed in Nb tubes.
Below two of the best apatite collected for this work (SL2_1, SL5_4).

CHAPTER 5

RESULTS

5.1 (U-Th)/He ANALYSIS

In this chapter the results of the (U-Th)/He analysis are presented and briefly commented. The detailed interpretation and discussion will be provided in the following chapter.

Among the 14 initial samples from Havis, only 4 contained apatites, furnishing a total of 5 crystals for the entire well. Among the 8 Salina samples, 4 were unproductive, the remaining samples provided 14 crystals of different qualities. The crystals were often quite abraded, slightly rounded and fractured perpendicular to the c-axis, but coating was generally minimal and a discrete part of the replicates was free of inclusions.

Name	H1	W1	H2	W2	morph. Index
HA1_1 AP	66,35	67,64	67,66	65,47	2
HA5_1 AP	152,42	85,81	154,11	75,5	1
HA6_1 AP	123,05	64,59	125,68	64,59	1,5
HA9_1 AP	129,5	61,89	126,98	58,52	1
HA9_2 AP	82,09	71,11	85,18	66,28	1,5
SL2_1 AP	179,01	75,99	181,44	68,79	1,5
SL2_2 AP	177	89,25	178,09	69,78	1
SL2_3 AP	190,34	90,16	195,04	78,33	1
SL5_1 AP	260,21	81,8	252,62	77,02	1,5
SL5_2 AP	155,52	90,1	157,47	85,26	1
SL5_3 AP	195,4	95,5	199,09	84,84	1
SL5_4 AP	192,18	77,54	194,67	75,54	1
SL5_5 AP	136,54	95,46	136,96	87,89	1
SL6_1 AP	118,07	83,83	124,84	89,03	1,5
SL6_2 AP	150,13	53,12	150,11	50,04	1
SL6_3 AP	163,72	59,27	165,47	59,26	1
SL6_4 AP	125,09	74,18	132,06	75,12	1,5
SL6_5 AP	189,77	83,45	191,76	93,38	1
SL7_1 AP	64,53	52,24	71,54	49,6	1,5

Figure 5.1 . The apatite prisms length and width measured parallel on the c-axis and the morphological index (1= intact crystal; 1.5= one missing ending; 2= two missing endings). The table shows all the measures performed on all the collected grains.

After the analysis, 2 crystals were discarded because of their critical analytical values. The dataset is displayed in the table in figure 5.2.

Grain n°	raw age (Ma)	±σ (Ma)	radius (µm)	U (ppm)	Th (ppm)	Sm (ppm)	^{4}He (nmol/g)	eU (ppm)	FT ^{238}U	FT ^{235}U	FT ^{232}Th	FT ^{147}Sm	fully FT correct. age (Ma)	±σ (Ma)
HA1_1	*0.29*	*0.04*	*35.57*	*61.94*	*2400.00*	*2317.29*	*1.00*	*625.95*	*0.62*	*0.57*	*0.57*	*0.87*	*0.51*	*0.07*
HA5_1	20.29	0.49	42.66	8.19	39.89	89.62	1.94	17.56	0.67	0.63	0.63	0.89	31.19	0.75
HA9_2	*1.66*	*0.41*	*36.06*	*9.61*	*60.02*	*220.18*	*0.22*	*23.71*	*0.62*	*0.57*	*0.57*	*0.87*	*2.81*	*0.69*
SL2_1	2.32	0.13	42.12	7.49	150.29	150.53	0.54	42.81	0.67	0.62	0.62	0.89	3.65	0.20
SL2_2	*12.05*	*0.25*	*43.25*	*22.44*	*119.33*	*34.69*	*3.30*	*50.48*	*0.68*	*0.63*	*0.63*	*0.89*	*18.47*	*0.37*
SL2_3	*2.31*	*0.12*	*46.00*	*15.73*	*90.00*	*88.60*	*0.46*	*36.88*	*0.69*	*0.65*	*0.65*	*0.90*	*3.44*	*0.18*
SL5_1	34.85	0.70	47.33	14.63	39.73	170.05	4.56	23.96	0.70	0.66	0.66	0.90	50.65	1.03
SL5_2	1.07	0.12	45.82	20.02	49.91	95.53	0.18	31.75	0.69	0.65	0.65	0.90	1.58	0.18
SL5_3	5.02	0.65	48.88	2.91	10.55	188.82	0.15	5.39	0.71	0.67	0.67	0.91	7.17	0.93
SL5_4	21.40	0.41	42.43	13.04	51.62	160.45	2.94	25.17	0.67	0.63	0.63	0.89	32.87	0.62
SL5_5	*3.32*	*0.35*	*46.14*	*9.00*	*21.88*	*189.75*	*0.26*	*14.14*	*0.69*	*0.65*	*0.65*	*0.90*	*4.86*	*0.51*
SL6_1	11.02	0.33	46.56	13.72	47.37	60.01	1.49	24.85	0.70	0.66	0.66	0.90	16.22	0.49
SL6_2	9.43	0.51	29.16	15.19	33.87	161.85	1.19	23.15	0.54	0.49	0.49	0.85	17.92	0.98
SL6_3	*1.96*	*0.76*	*33.29*	*11.57*	*16.73*	*94.89*	*0.17*	*15.51*	*0.59*	*0.54*	*0.54*	*0.87*	*3.39*	*1.31*
SL6_4	5.10	0.22	41.52	18.85	84.50	141.06	1.07	38.71	0.66	0.62	0.62	0.89	7.94	0.35
SL6_5	4.07	0.16	47.82	9.93	56.53	44.14	0.51	23.21	0.70	0.66	0.66	0.90	5.98	0.24
SL7_1	20.45	0.92	27.19	25.95	82.82	295.29	5.07	45.41	0.52	0.46	0.46	0.84	41.44	1.86

Figure 5.2 . Complete results dataset of the analysis. In the table are not shown the discarded crystals. Italic highlights data with anomalous values.

The results clearly show a very low reproducibility of the ages which are highly scattered, even among crystals from the same sample. These variations are apparently not related to a wrong choice of grains as all the analyzed crystals were of good quality.

The outcomes of the analysis are summarized for each sample as follows:

→ *HA1* exhibits a very low fully corrected age due to an anomalously high content in U, Th and Sm, noticeable also in the extremely high value of eU.

→ *HA5* presents a crystal without any anomalous data. Nevertheless the corrected age is quite old if compared to the mean of the other data.

→ *HA9* shows a quite low ^{4}He content that could have produced inaccurate evaluations.

→ *SL2* displays three good data. An excellent age convergence is visible only on two crystals out of three. Reproducibility is poor.

→ *SL5* exhibits two anomalous data, out of five, because of a low ^{4}He content. Age reproducibility is particularly low, the ages spanning from 50.65 Ma to 1.58 Ma (the maximum and one of the minimum values detected among all the analyzed samples).

→ *SL6* shows only one anomalous analysis, once more due to a poor quantity of ^{4}He. Age reproducibility is low, but the differences are less pronounced then other samples.

→ *SL7* presents only one crystal. No odd data are noticeable, anyway the calculated corrected age is far from rough mean of the other values.

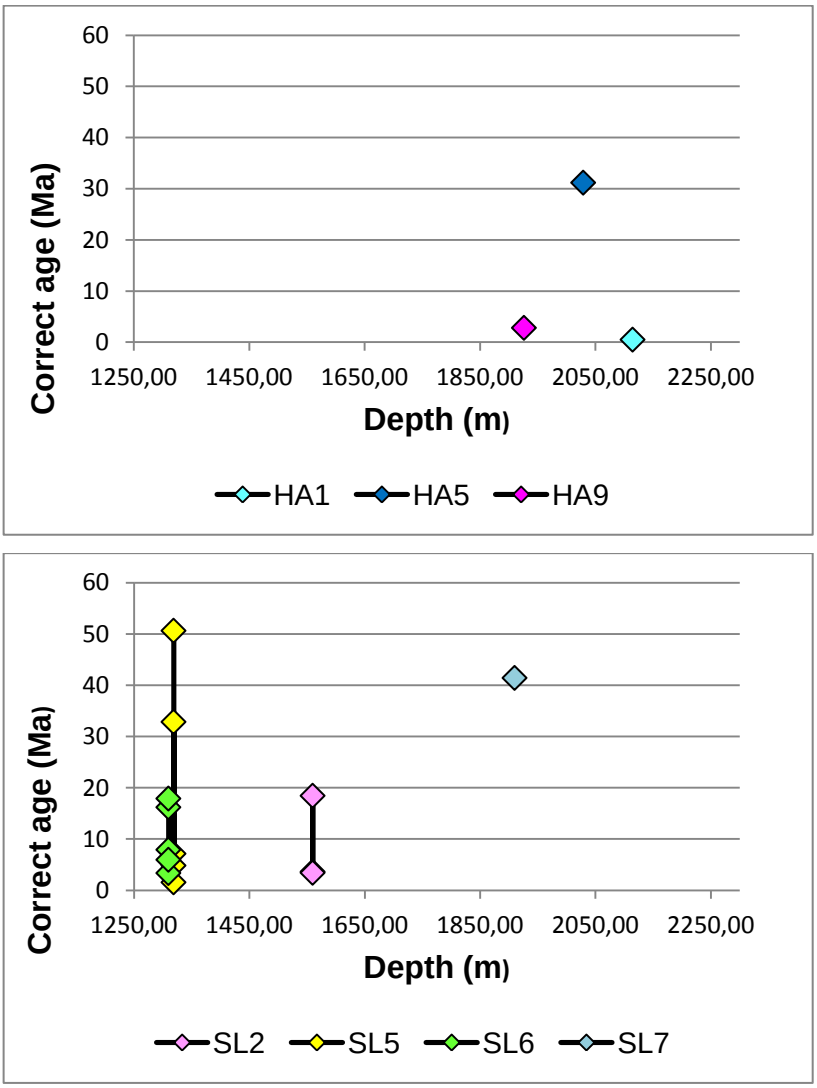

Figure 5.3 . Samples from Havis and Salina have been divided into two different graphs. Age vs. depth is represented in order to highlight the strong data dispersion and the weak bound between age and depth of samples.

U-Th/He dating is based on the assumption that the ^{4}He ingrowth depends only of the age of closure of the system. Therefore, the age should not depend by the chemistry of the apatite crystal. In order to verify this assumption, a graphics can be plotted, in order to check the relationship between age and eU content.

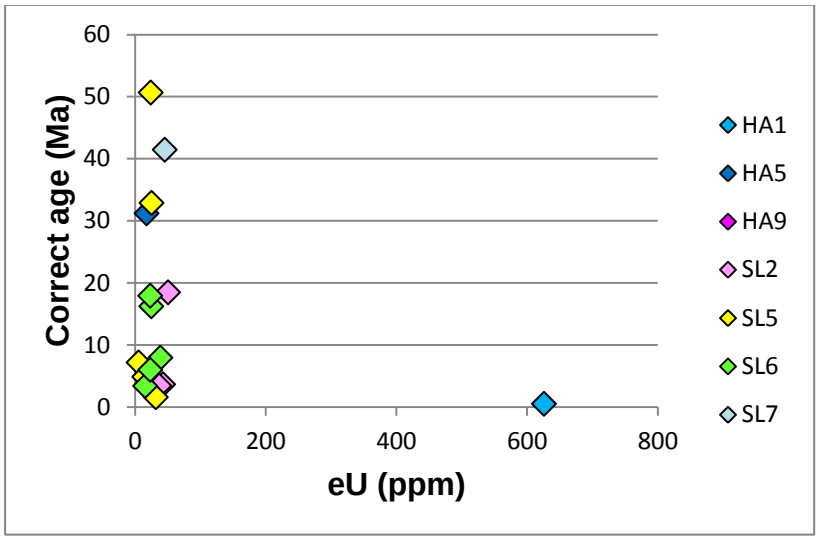

Figure 5.4 . Relationships between age and effective Uranium content (eU) is shown in the graph. All the samples, both from Havis and Salina, are plotted.

Data appear to be slightly scattered, and it is not visible any correlation between results and analytical values, therefore the measured age can be considered not affected by problems related to the chemistry of the crystals. Only sample HA1 exhibits an anomalously high effective Uranium content so the age data for this sample cannot be considered fully reliable.

5.2 MODELLING PROCEDURE

5.2.1 SIMBA SOFTWARE

In order to provide a complete dataset of the modelling procedures, SIMBA software packet will be discussed as follows. This procedure, performed by ENI operator, was divided into multiples steps.

1) *Grid2mod*

This first stage aims to produce 3D structural maps starting from seismic data and correlations between wells' data.

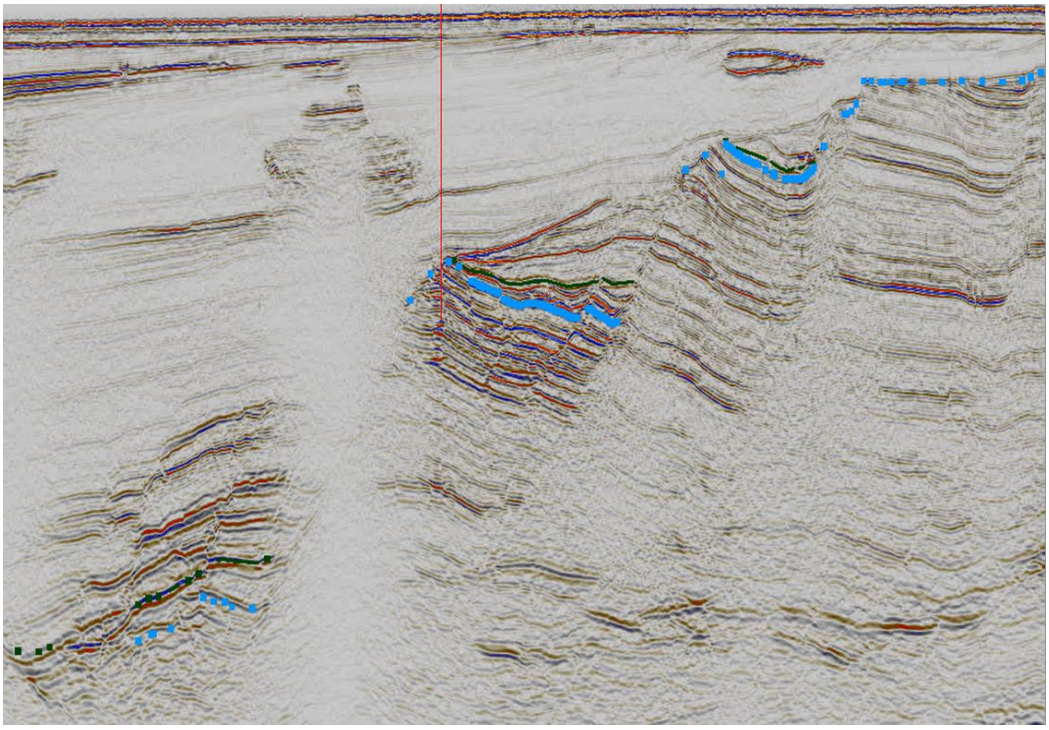

Figure 5.5 . Seismic profile. The sketch shows a W-E section. The red vertical line indicates the Havis well position. Light blue and dark green dots mean to identify the bottom and the top of the reservoirs. Wavy red lines show the main unconformities.

The image in figure 5.5 shows an example of a 2D seismic profile partially interpreted. The reservoir layer on the right part of the sketch, that is the westernmost part of the structural high (Loppa High), is correlated with some

of the top horizons of the three tilted blocks on its left. Next to the west side of the well, information has been lost because of the presence of a gas full cavity at a quite shallow depth that erased all the seismic data below it. By the means of Grid2mod software a 3D model was then produced. Figure 5.6 shows only the main identified layers that describe the present day setting beneath the Barents Sea seafloor.

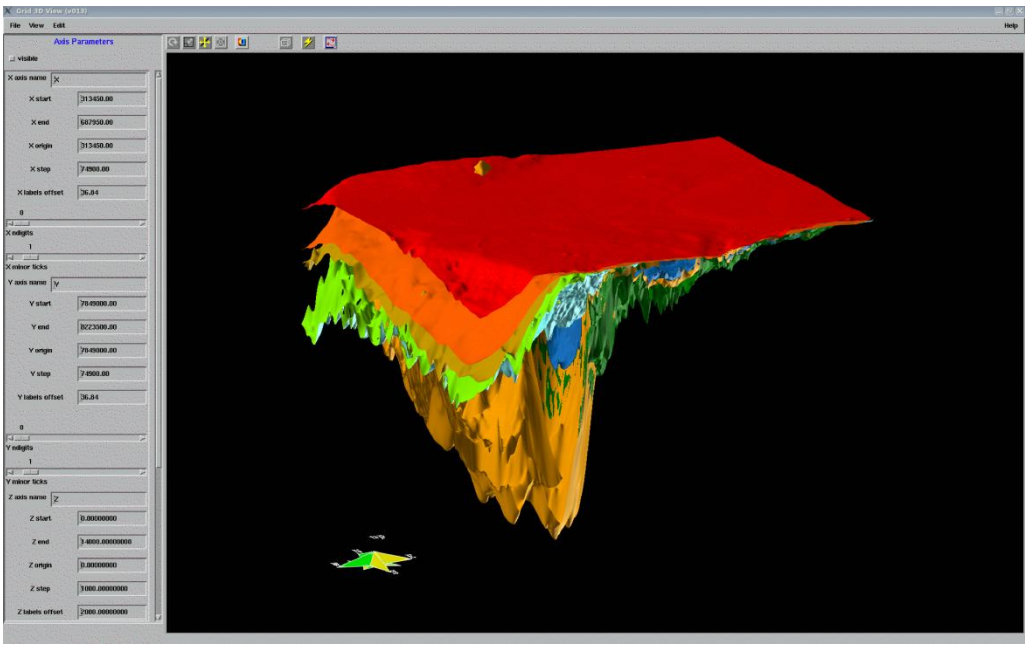

Figure 5.6 . Snapshot of a Grid2mod frame. Z-axis scale has been exaggerated to better show the different layers.

2) *Basin Scenarios*

The part of the process developed with this software aims to assign specific age and features to each layer. By this stage a geological background is given to the model.

3) *Geo Restore*

This SIMBA software element allows to reconstruct the basin history through time. Compaction curves are estimated starting from the layers properties and thicknesses; also the palaeobathimetry has been estimated and considered by the means of biostratigraphical studies. Therefore, Geo Restore provides 3D models of the basin during each stage of its evolution, considering thicknesses variation due to compaction and the deformation of the layers due to the

depositional load (figure 5.7). Thanks to this reconstruction burial histories can be developed (as shown in figures 5.8 and 5.10).

4) *Tempra*

This later step aims to hypothesize the evolution of temperatures and pressures during the basin evolution. A rough thermal history is therefore produced. As it will be state in the next paragraph, this is one of the basic starting points to develop a far more accurate and precise thermal histories that will lead to the resolution of the scientific aim of this work.

5) *Generation&Expulsion* and *Hydrocarbon Migration*

This is the last phase of the SIMBA software process. By the means of this package of software hypothesis about the nature and the moves of the hydrocarbon resources can be made.

5.2.2 HeFTy SOFTWARE

After the samples analysis, data have been modelled in order to reconstruct the thermal history of the area. Many thermal histories have been generated using the software described in Chapter 3: "HeFTy". First of all, it was necessary to select the available crystals for the modelling. As stated in the previous paragraph, not all the analysed apatite produced straightforward results, therefore some of them have been set aside and not further used. During this first selection the discarded crystals were: HA1_1, HA5_1, SL5_1, SL5_4, SL6_1, SL6_2, SL7_1. The choice has been done considering the fully corrected age produced by the analysis and the geological and tectonic context, already described in Chapter 2. The modelling procedures were then performed on the remaining crystals.

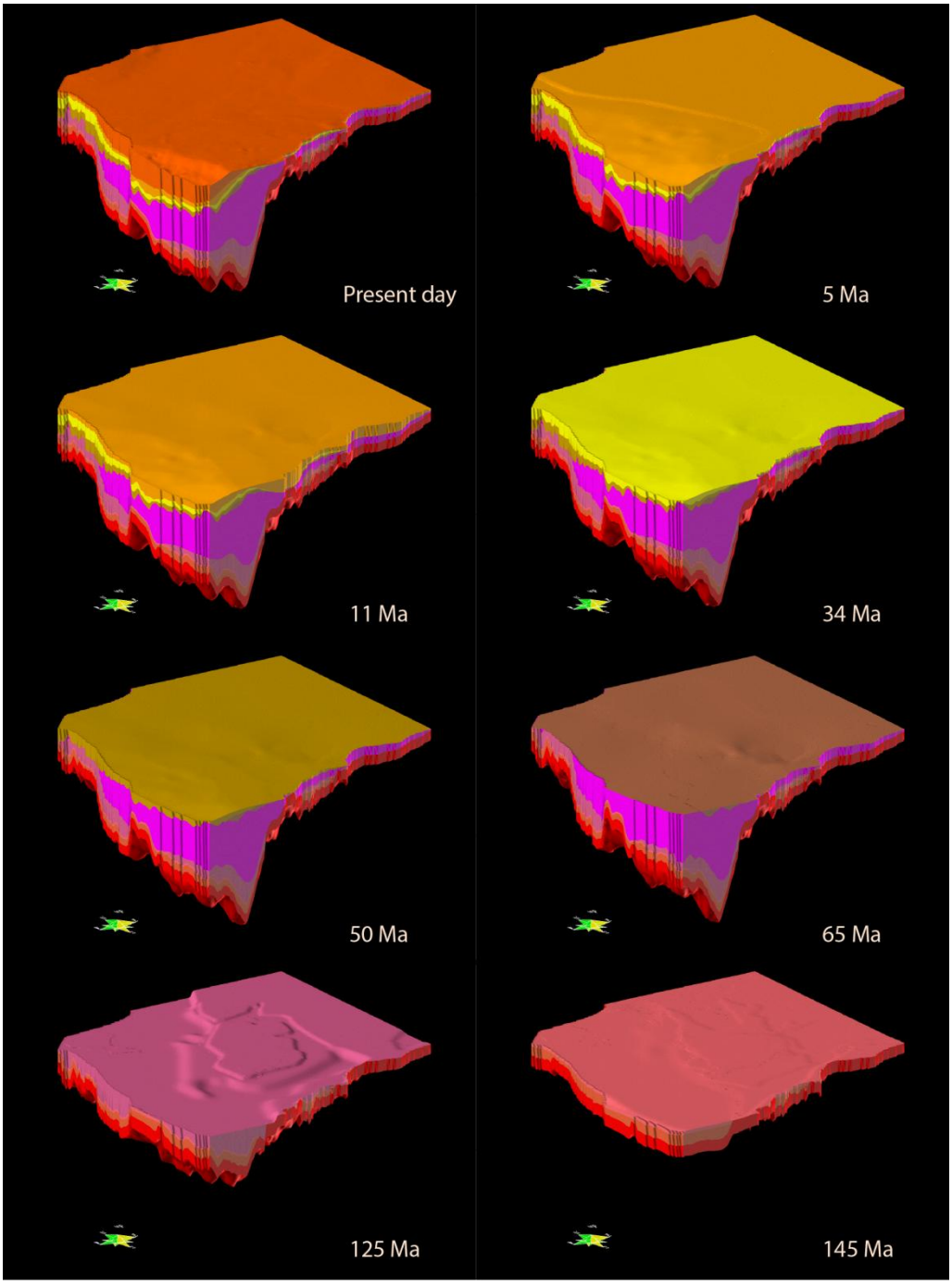

Figure 5.7 . Reconstruction of the basin evolution produced with Geo restore software. The evolution is represented starting from the present day situation to nearly the origin 145 Ma. Decompaction is noticeable.

Given the burial histories of the wells, the vitrinite reflectance data and the related temperature evolution, have been used to constrain the modelling procedure (figure 5.8). HeFTy constraints consist in boxes which give the software a range of good temperatures for a determined period of time. For each model, seven to ten boxes were used to reproduce correctly the burial data. To avoid miscomprehensions, it is important to underline that the temperature sketch provided by the burial histories would not be adequate to distinguish the precise timing of the exhumation and, as a consequence, to reconstruct the Cenozoic tectonic evolution. A more accurate technique, such as a careful thermal history modelling, was absolutely necessary to reach the aim of the study. A quantitative evaluation of the thermal history was so performed to find a range of cooling paths compatible with thermochronology data. In this work, inverse modelling of (U-Th)/He data was performed by generation of possible T–t paths by a Monte Carlo algorithm.

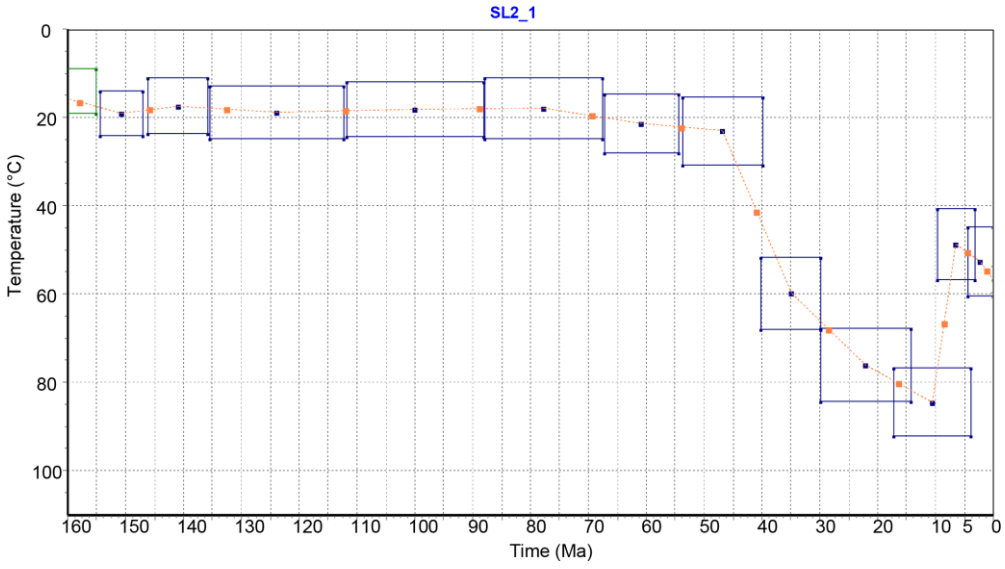

Figure 5.8 . Frame from HeFTy software. The image shows the constraints path developed on the thermal evolution inferred using Tempra from SIMBA software.

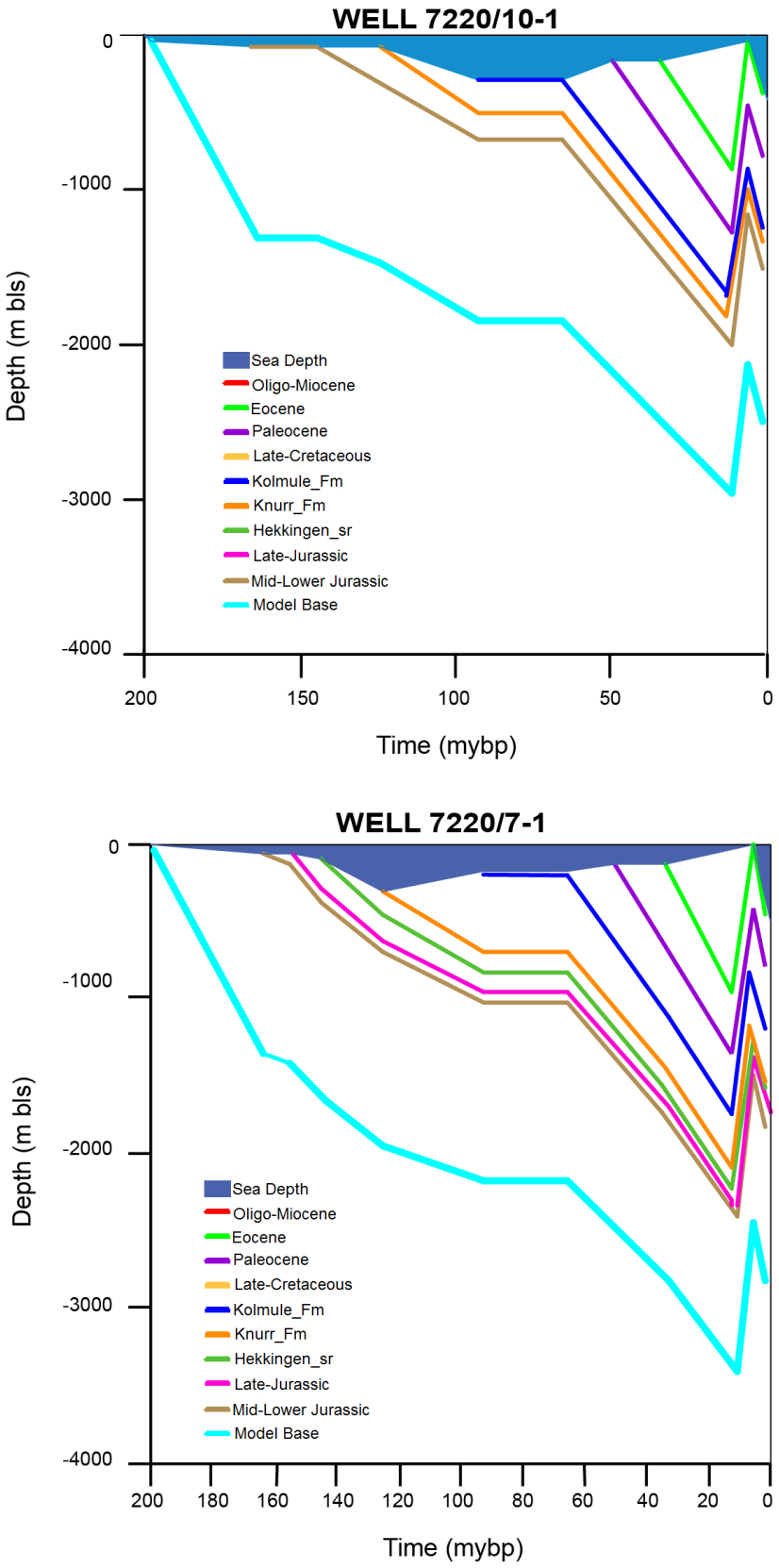

Figure 5.9 . Burial histories of Salina (well 7220/10-1) and Havis (well 7220/7-1).

Initially the software was asked to provide a total of 10.000 paths, both acceptable and good, following the imposed constrains. Not all the crystals brought to this stage produced satisfying results compatible with the thermal tracks. Only three apatites were considered optimal: SL2_1, SL2_3 and SL5_5. For these samples, a more accurate stage of modelling was carried on. During this second step, HeFTy was asked to provide a minimum of 30 good paths for each model, taking a longer calculation time. Once more all the three crystals gave straightforward results.

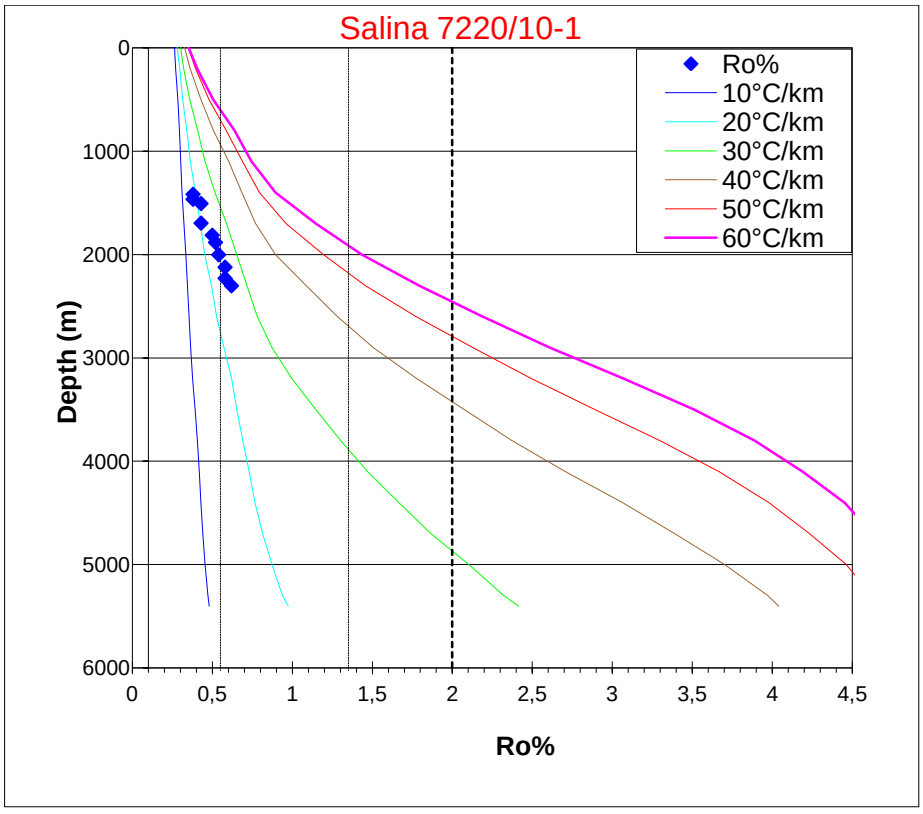

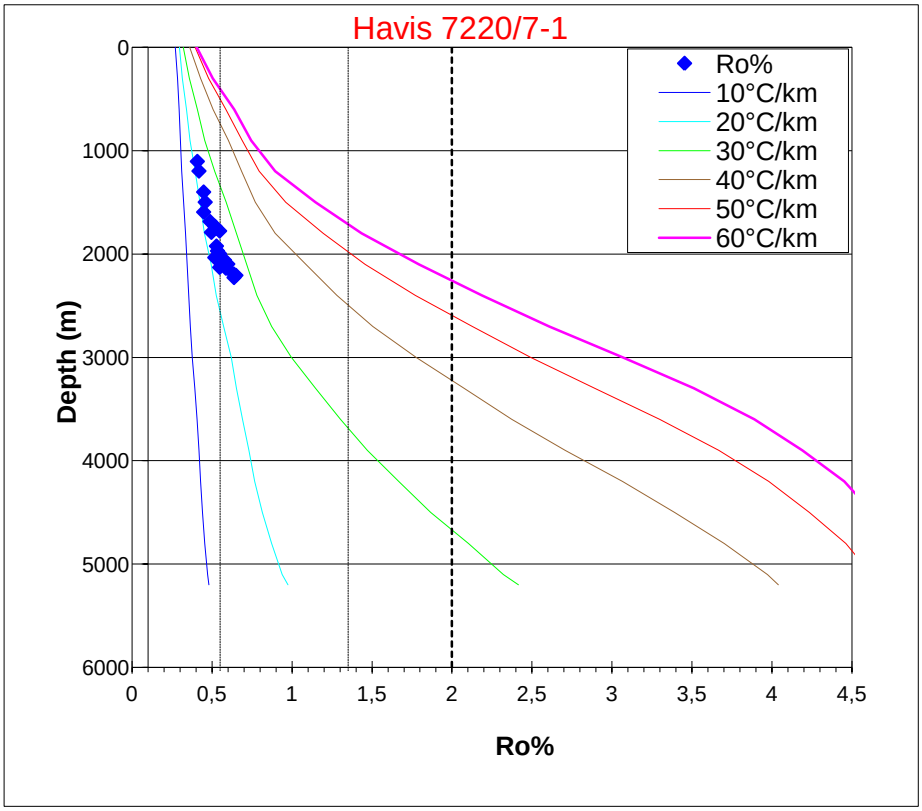

Figure 5.10 . Measured vitrinite reflectance is plotted in the graphs. Thermal gradient is shown.

In order to provide a complete overview on the dataset used for this study, data and burial history from the well 7220/5-1 (Skrugard), elaborated during a companion project at the Department of Geosciences, will be shown. In the next chapter, data from this core will be discussed alongside with well 7220/10-1 and well 7220/7-1 data to deal with complete and significant comparisons.

Grain n°	raw age (Ma)	±σ (Ma)	radius (µm)	U (ppm)	Th (ppm)	Sm (ppm)	^{4}He (nmol/g)	eU (ppm)	FT ^{238}U	FT ^{235}U	FT ^{232}Th	FT ^{147}Sm	fully FT correct. age (Ma)	±σ (Ma)
SK_1	2,13	0,16	36,45	5,99	47,2	27,42	0,2	17,08	0,62	0,58	0,58	0,88	3,6	0,27
SK_2	2,01	0,1	42,92	9,16	32,94	36,51	0,18	16,9	0,63	0,63	0,63	0,89	3,08	0,16
SK_3	3,8	0,22	34,05	11,49	24,21	27,25	0,35	17,18	0,6	0,55	0,55	0,87	6,52	0,38

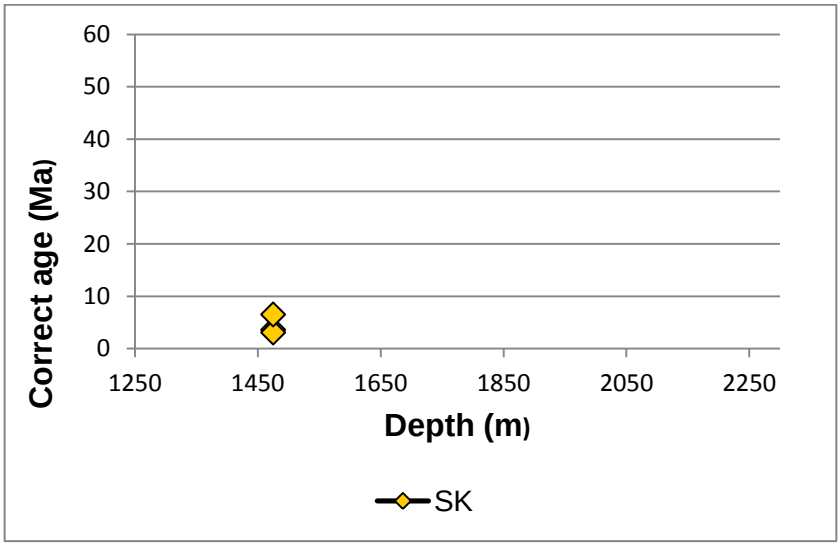

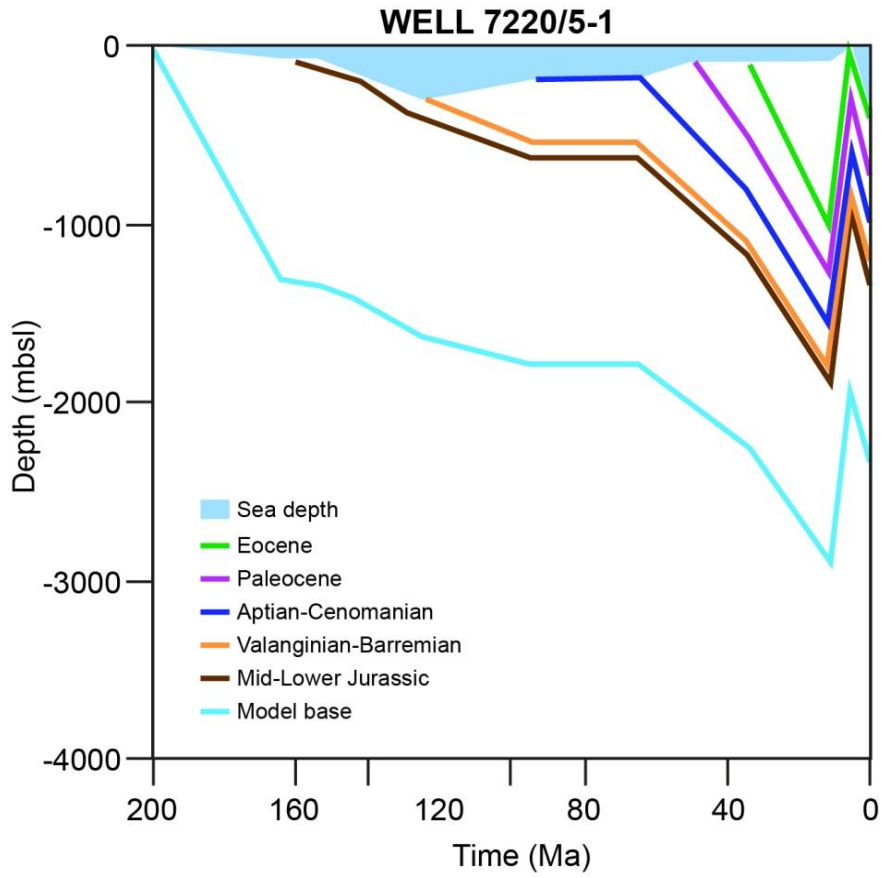

Figure 5.11 . In the table are displayed the data from the analysis performed on apatite of well 7220/5-1 (Skrugard). Below: (1) the graphic shows data dispersion; (2) burial history of Skrugard.

CHAPTER 6

DISCUSSION

Given that most of the analyses can be considered reliable, data clearly show that all the single grain ages are far younger than depositional ages, thus indicating a total resetting after deposition. Because of the high dispersion previously shown, a relationships between depth and ages could be anyway expected, being the deepest samples cooled later below the closure temperature. These relationships are not clear in the wells 7220/10-1 and 7220/7-1 but are much more evident in the well 7220/5-1. The weak age-depth correlation and the large spread of single ages may suggest a long permanence in the Partial Resetting Zone or, at least, maximum temperatures which are not far exceeding the total resetting temperature. As a consequence, small variations in the apatite kinetics result in a large variation of ages. Vitrinite values increase with depth as expected but they are in the immature stage (Ro<0.6%) for the sampled depths. Sedimentary evolution is characterized by nearly continuous burial from Jurassic to the Miocene, later an erosion phase started during the end of Miocene and then a final burial to present depth. Two main depositional hiatus are recognizable: between (1) Jurassic and Cretaceous sequences and between (2) Cretaceous and Cenozoic series. The total erosion was estimated by studying the glaciogenic sediments deposited on the Barents shelf between 2,7 and 0,7 Ma. Using appropriate assumptions and corrections linked to the features of the source rock and the compaction of the erosional products, the total volume of deposited sediments has been evaluated between $135 \cdot 10^3$ Km^3 and $99 \cdot 10^3$ Km^3 (Laberg et al., 2012). Other recent studies (Henriksen et al., 2011) aimed to calculate the erosion value in order to estimate the extent of the phenomenon. According to the resulting model, developed starting from Henriksen et al. (2011) simulation, from 700 m (close to well 7220/10-1 Salina) to 1000 m (close to the Havis site) were eroded, in the area of interest, during the uplift phase. The maximum temperatures

reached by sampled sediments were on the order of 80-90°C, therefore matching well with the thermochronological results as they prove that reset of the U-Th/He was nearly complete.

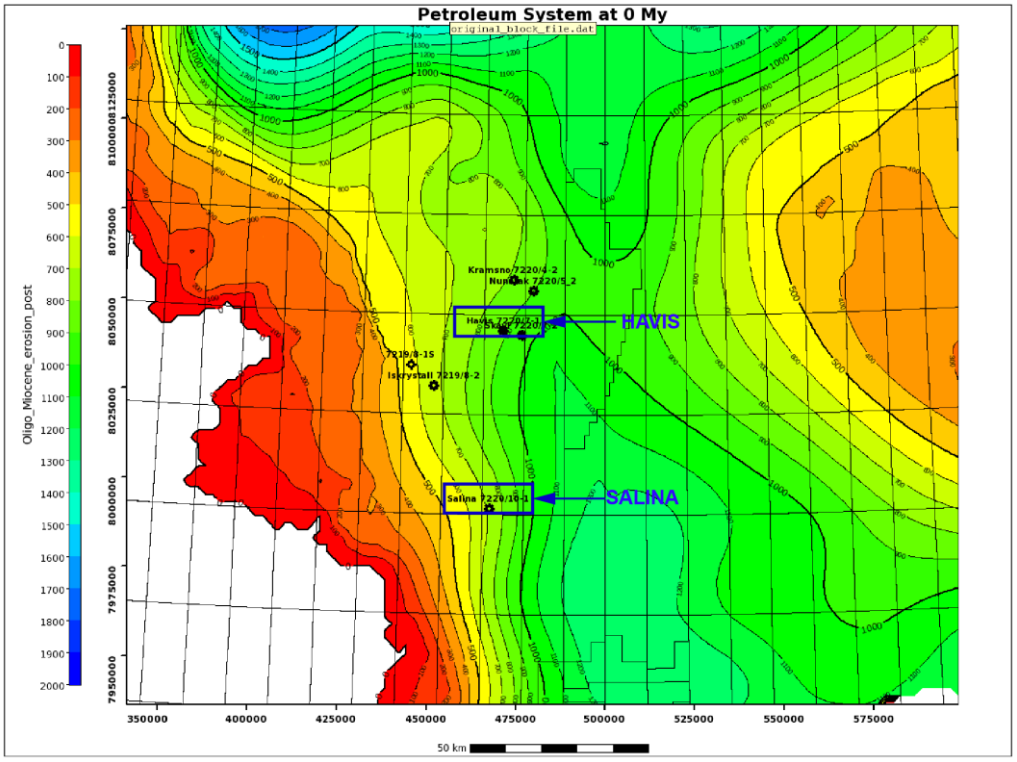

Figure 6.1 . Resulting model for the erosion estimation. Erosion for Salina is lower than the Havis site. Moving from the studied wells sites, it is noticeable that a maximum erosion involved the structural highs on the eastern and the northern parts. Moving westward, from the shelf to the basin, no erosion evidences were recorded. (modified from Henriksen et al., 2011)

Actually, as already asserted, the precise timing of basin inversion can be resolved only through thermochronological data. The colored envelope on figures 6.2 and 6.3 in the graphs indicates the confidence area defined by all the good paths processed by the software; within this paths envelope results can be considered adequately good. Each sketch presents two model lines: (1) the black dotted line represent the best result obtained by the software to describe the thermal history of the crystal: anyway, sometime, these models are meaningless from a geological point of view, as they are only based on a statistic calculation; (2) the blue continuous lines represent a mean

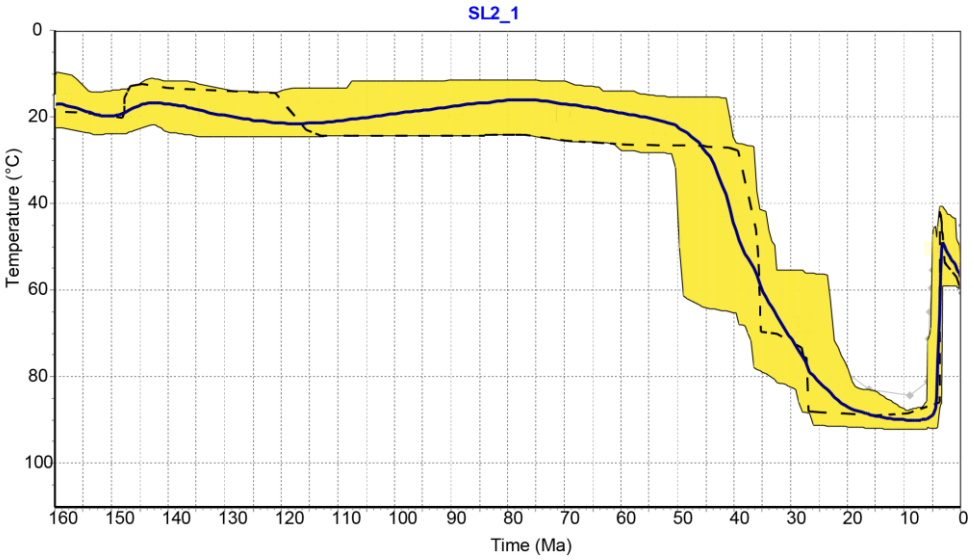
SL2_1
Temperature (°C)
0
20
40
60
80
100
160 150 140 130 120 110 100 90 80 70 60 50 40 30 20 10 0
Time (Ma)

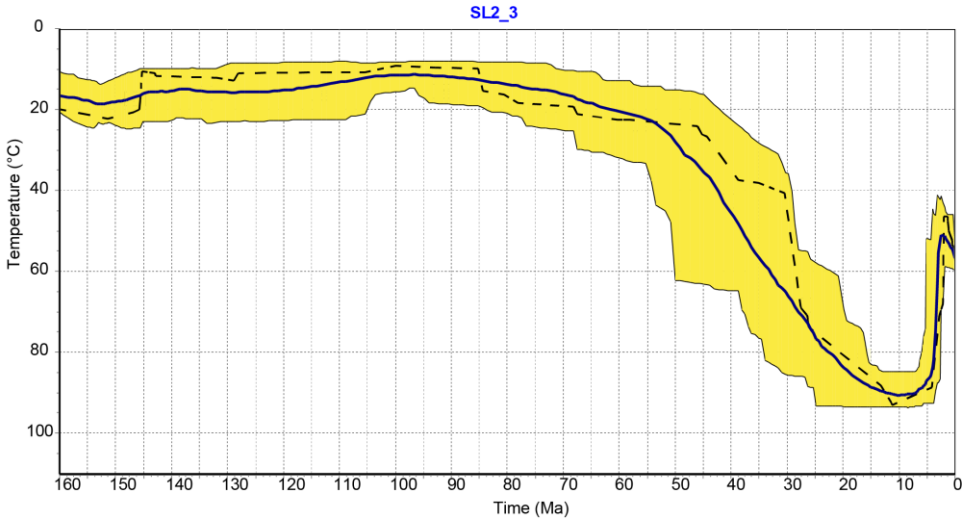
SL2_3
Temperature (°C)
0
20
40
60
80
100
160 150 140 130 120 110 100 90 80 70 60 50 40 30 20 10 0
Time (Ma)

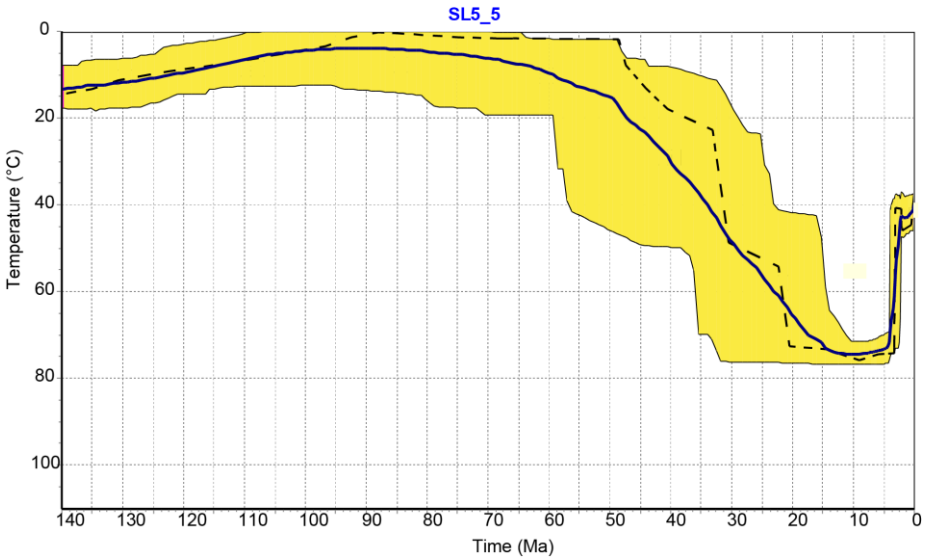
SL5_5
Temperature (°C)
0
20
40
60
80
100
140 130 120 110 100 90 80 70 60 50 40 30 20 10 0
Time (Ma)

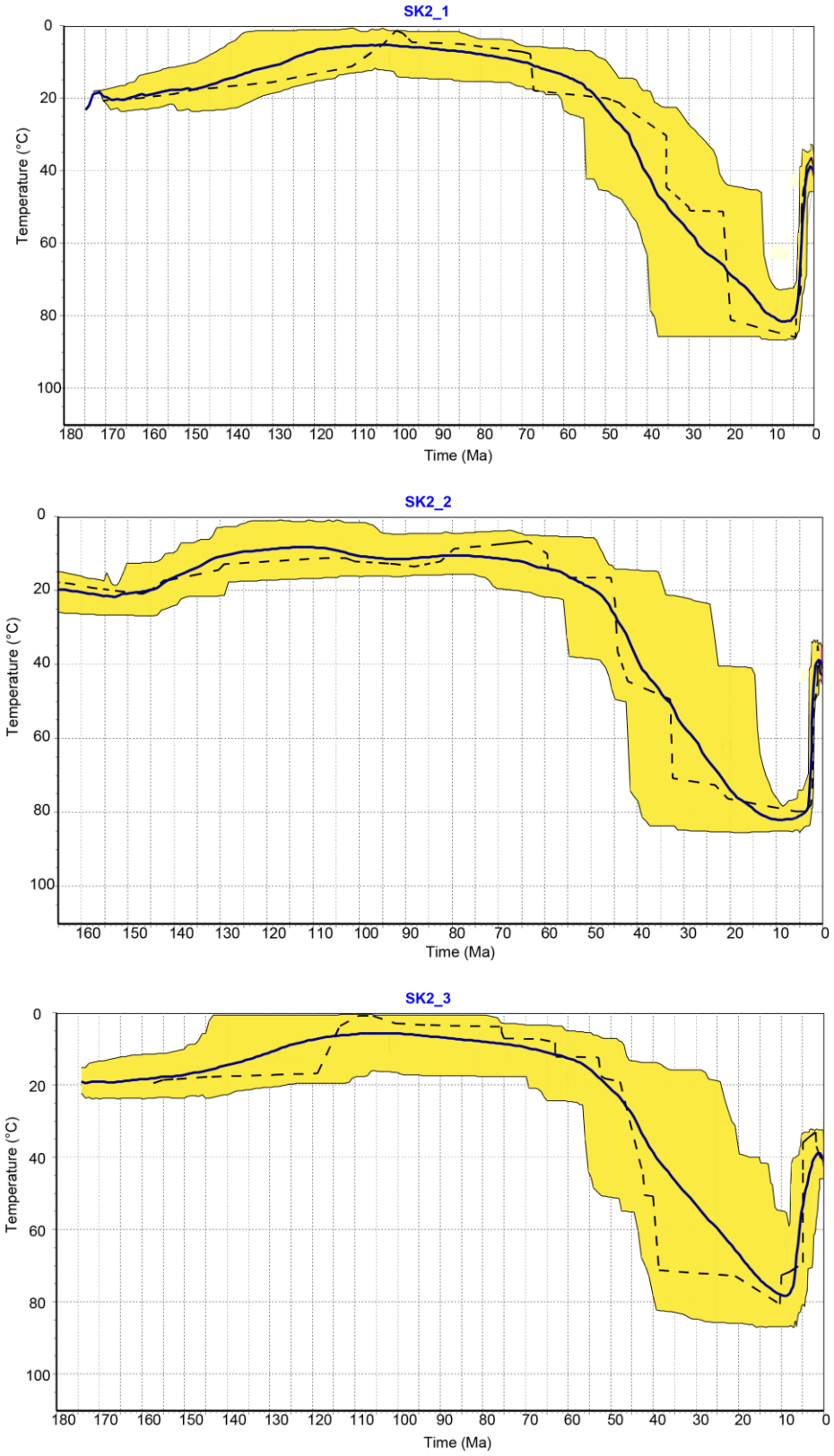

Figure 6.2 . HeFTy elaborations show the entire thermal evolution of the area starting from the selected crystals.

of all the good paths calculated by HeFTy. For almost all the simulations GOF is higher than 0.8, thus indicating a good fit between experimental and predicted results. Since the exhumation that this work aims to investigate is quite recent, we focus on the last 40 million years (figure 6.3).

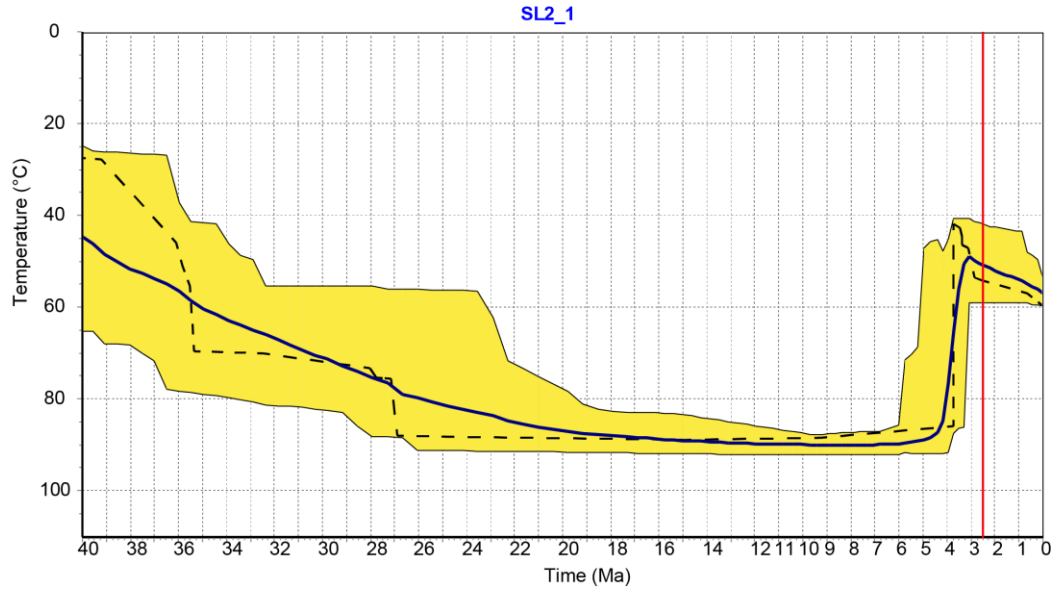

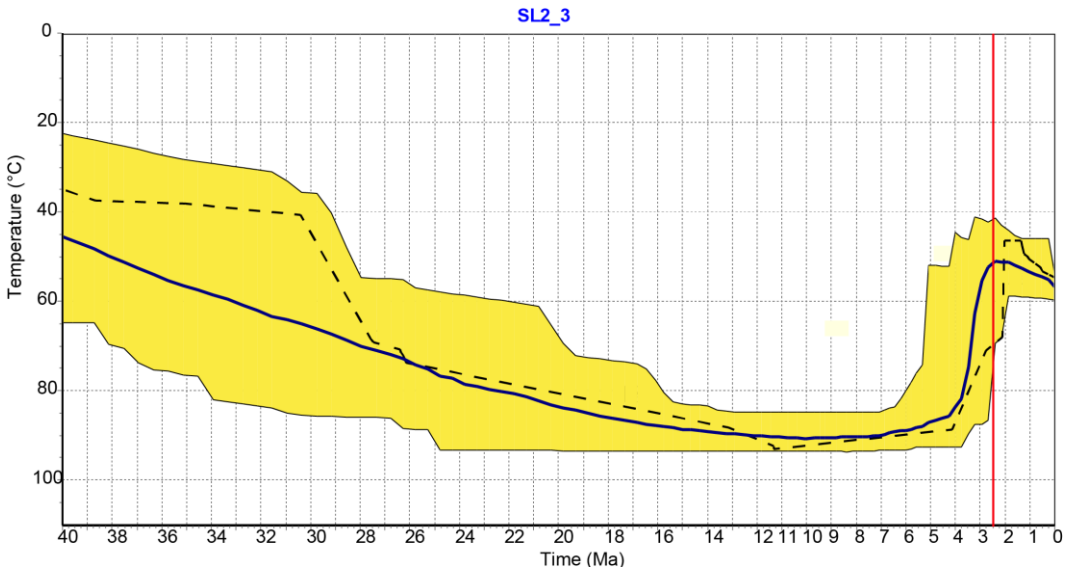

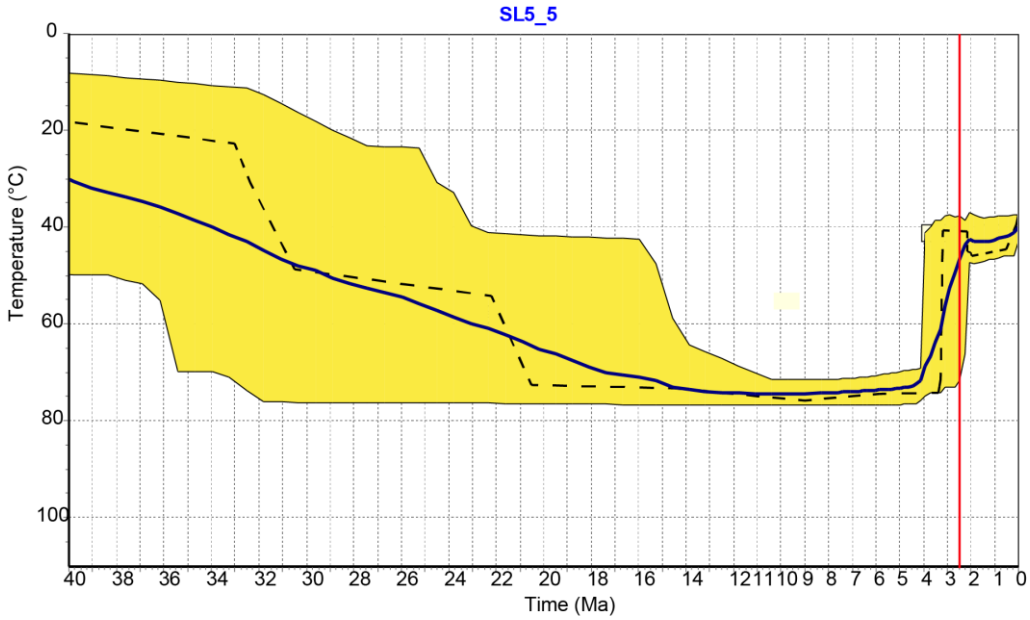
SL5_5
Temperature (°C)
0
20
40
60
80
100
40 38 36 34 32 30 28 26 24 22 20 18 16 14 12 11 10 9 8 7 6 5 4 3 2 1 0
Time (Ma)

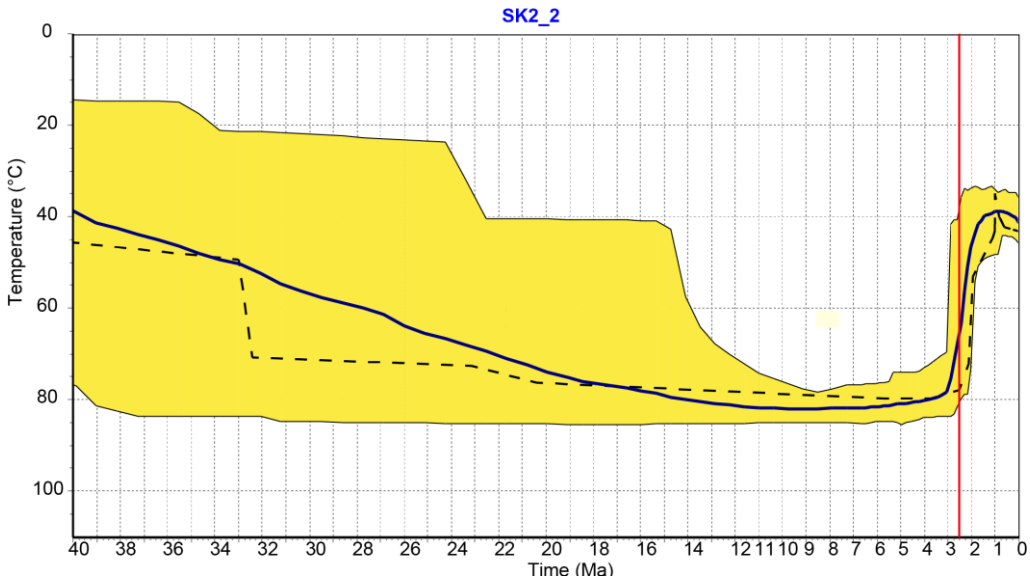
SK2_2
Temperature (°C)
0
20
40
60
80
100
40 38 36 34 32 30 28 26 24 22 20 18 16 14 12 11 10 9 8 7 6 5 4 3 2 1 0
Time (Ma)

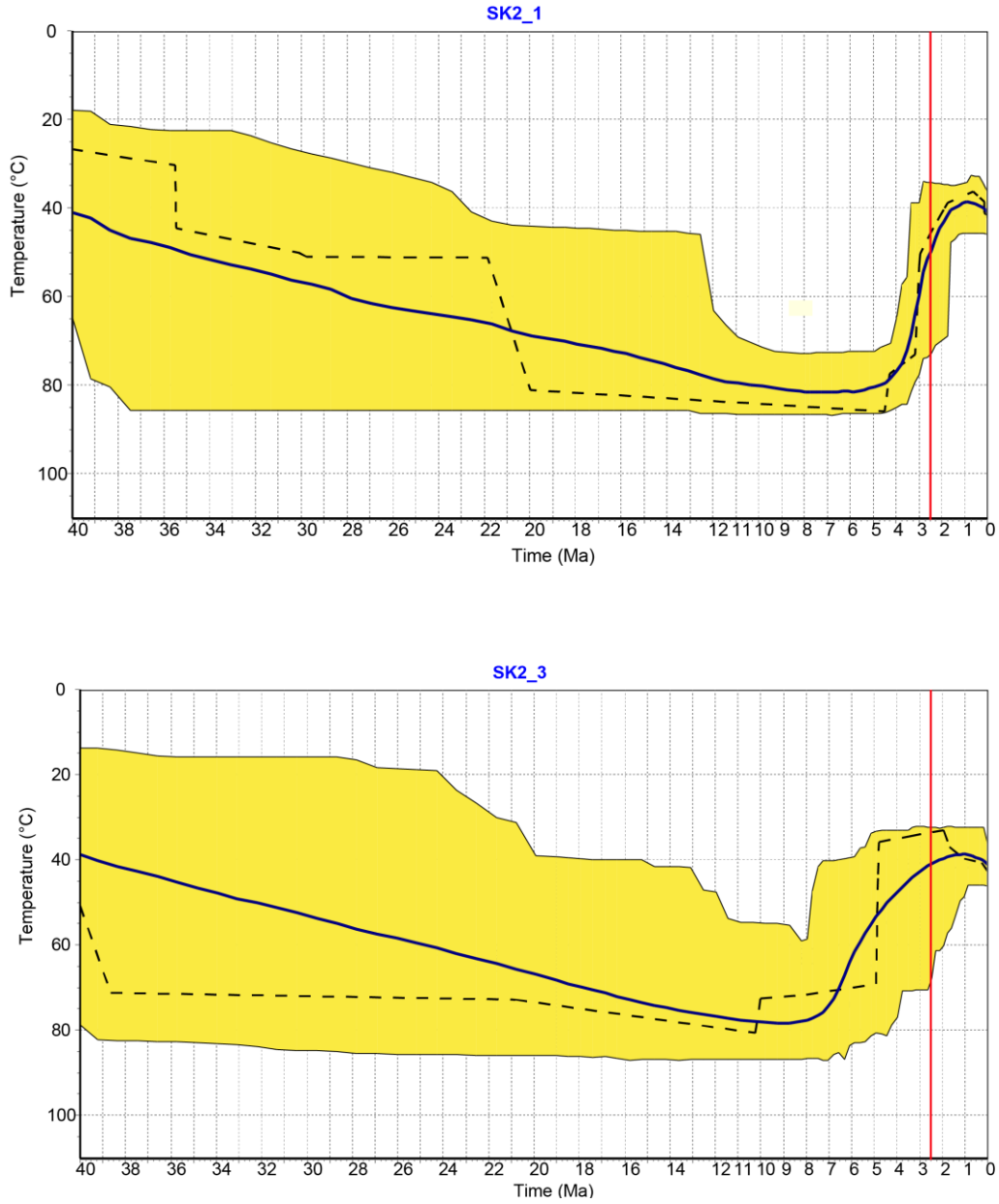

Figure 6.3 . The last 40 million years are displayed in the figures. The red vertical line marks the beginning of the glacio-fluvial activity that involved the Barents Sea during Cenozoic.

All the six crystals recorded three main evolution stages: a long burial period, from Jurassic to Miocene, a Cenozoic exhumation and then a new burial process. The evidences collected from this analysis show that time of final exhumation was antecedent to the period when the glacio-fluvial activity begun to shape the Barents Sea area. The recorded uplift started between a maximum of 8 Ma and a minimum of 6 Ma. Given these results, uplift triggered mainly

by ice-sheets erosion is not far acceptable. Nevertheless, this idea was already weakened by the fact that the shelf was shaped by ice-sheets while it was beneath the sea level, therefore ice masses activity had necessarily to be weaker, due to the Archimedes floating principle, than a subaereal activity, that theoretically could have produced the measured amount of erosion.

6.1 PETROLEUM SYSTEM

In the drilled area source rocks are estimated to be the top Jurassic of Hekkingen Formation, for well 7220/10-1 (Salina), and the mud levels beneath Stø Formation in Havis site. After generation and maturation processes hydrocarbon necessarily migrated to the traps. In this particular case strata where hydrocarbons are supposed to be stored are older than the sources. This peculiarity is due to the local tectonic evolution. Extensional tectonic events broke up the Loppa High margins; as a consequence, the subsurface is now organised in a series of tilted blocks separated by normal faults and overlaid by more recent sediments (as visible in figure 5.5). Hence, this evolution produced, for some of the blocks, adequate burial to bring source strata to the hydrocarbon generation stage and then migration was favoured by faults and permeable layers. Due to their low density, gas and oil move upward driven by a buoyancy pressure. In this area the possible traps filling processes are: (1) firstly mature hydrocarbons could have moved from the source rock through the permeable fault that allowed the resources to accumulate on the top of the adjacent tilted block sealed by fine grained sediments; (2) secondly hydrocarbons could have just moved upward vertically because of a seals failure, due to a pressure variation. This change was reasonably triggered by a tectonic event such as the exhumation stage just inferred by the experimental data. In this second case, oil and gas moved upward until they run into a new compact seal that avoided any further vertical migration and pushed the hydrocarbons laterally, to the top of far tilted blocks.

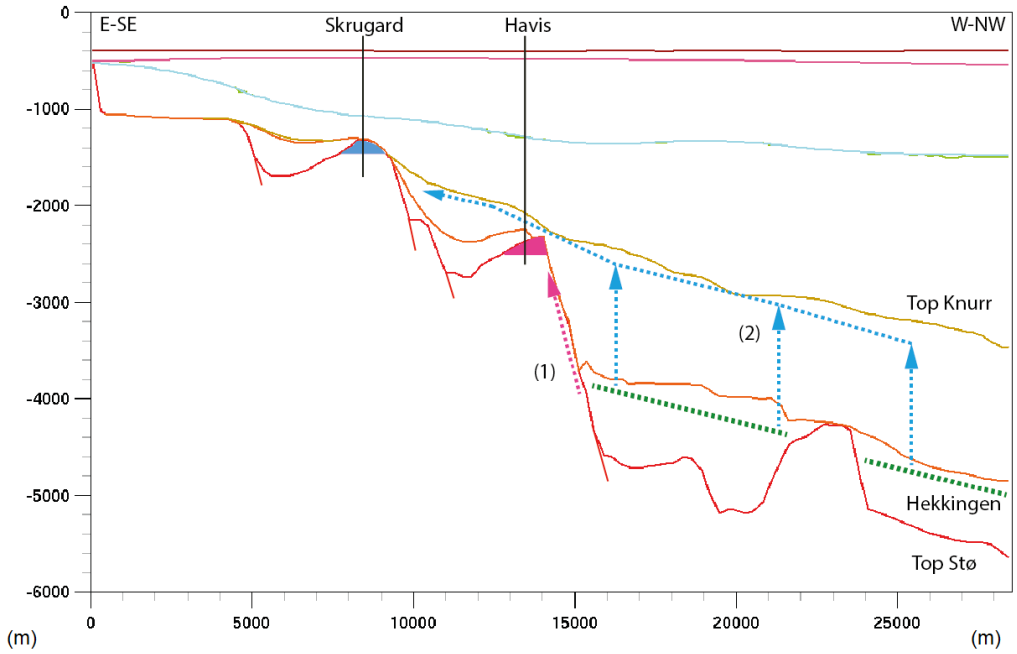

Figure 6.4 . The figure schematise the two possible filling processes described in paragraph 6.1 .

CHAPTER 7

CONCLUSION

Different models have been proposed to explain the last uplift event that interested the Barents Sea shelf. Data based on model assumptions, such as the net erosion of the area, find positive confirmations in the experimental measurements performed for this study, validating the widely accepted appraisals. On the contrary the timing of the event is a controversial topic. Evidences were so obtained by low temperature (U-Th)/He thermochronological method on apatites. Procedures for the samples preparation, the cataloguing of the selected crystals and then the processing of obtained data were performed accurately and in compliance with the carefulness, assumption and methodologies accepted for this kind of analysis; therefore results can be considered significant. Experimental data show consistent results, with the beginning of the uplift that can be so estimated at 7 ±1 Ma. This evidence allowed to discard the hypothesis which considered this exhumation event as a glacio-fluvial erosion consequence. As a consequence the causes of the uplift need to be sought in a tectonic context. Indeed, during the opening of the Atlantic ocean, and so far of the Norwegian-Greenland Sea, multiple strike-slip faults generated on the Barents Sea western margin. It could be therefore probable that the area was locally subject to compressional regime stresses; this situation could have produced the opportune conditions to induce uplift and erosion that mainly involved the structural highs, such as the Loppa High.

ACKNOWLEDGMENTS

I would really like to thank all the people who helped me during my Master Thesis work. First of all Prof. Massimiliano Zattin and Dr. Benedetta Andreucci that taught me, step by step, every day, everything they know. Then I would really love to thank Dr. Domenico Grigo who helped me, not only for the completion of my paper, but even for letting me breath the atmosphere of one working day inside the oil company. I'd also like to thank Dr. Filippos Tsikalas for the kindness and willingness that demonstrated to us during our visit to Norway. Last but not least I would like to thank Dr. Sandra Boesso who carefully assisted me during my lab experience and even fed me with good music and dark chocolate cakes. Now I cannot forget to thank all the special people who supported me outside the University environment. I need to thank my parents, who are the most enthusiastic about my work. My mother, who is so much proud of me, and my father, for his never ending search for "plan b" to always have one more chance to succeed. *Dulcis in fundo*, I would really love to thank my superspecial man Paco who supported me whatever my choice was, maybe because he always knew that all of this "would have been a success". And then I am going to close this free page of acknowledgments thanking all those tens of people that, one way or another, helped me to be the person I become. Hopefully from my last days as a master student, over and out.

REFERENCES

ANDREUCCI B., 2013 *Thermochronology of the Polish and Ukrainian Carpathian,* PhD Thesis

BJOROY M., HALL P.B., FERRIDAY I.L., MORK A., 2010 *Triassic Source Rocks of the Barents Sea and Svalbard,* Search and Discovery article, AAPG Convention, Denver, Colorado

CARR A.D., SCOTCHMAN I. C., 2003 *Thermal history modelling in the southern Faroe–Shetland Basin,* Petroleum Geoscience, vol. 9, p. 333–345

CAVANAGH A.J., DI PRIMIO R., SCHECK-WENDEROTH M., HORSFIELF B., 2006 *Severity and timing of Cenozoic exhumation in the southwestern Barents Sea,* Journal of the Geological Society, v.163; p761-774

DENGO C.A., RØSSLAND K.J., 1992 *Extensional tectonic history of the western Barents Sea,* Structural and Tectonic Modelling and its Application to Petroleum Geology, p91-107

DORE' A.G., 1995 *Barents Sea Geology, Petroleum Resources and Commercial Potential,* Arctic, vol. 48, no.3 p207–221

DORE' A.G., LUNDIN E. R., FICHLER C., OLESEN O., 1997 *Patterns of basement structure and reactivation along the NE Atlantic margin,* Journal of the Geological Society, vol.154; p.85-92

DORE' A.G., LUNDIN E.R., JENSEN L.N., BIRKELAND Ø., ELIASS P. E., FICHLER C., 1999 *Principal tectonic events in the evolution of the northwest European Atlantic margin*, Petroleum Geology of Northwest Europe: Proceedings of the 5th Conference, 41- 61.

DORE' A.G., JENSEN L.N., 1996 *The impact of late Cenozoic uplift and erosion on hydrocarbon exploration: offshore Norway and some other uplifted basins,* Global and Planetary Change, vol.12 p. 415-436

DÖRR N., LISKER F., CLIFT P.D., CARTER A., GEE D.G., TEBENKOV A.M., SPIEGEL C., *2012 Late Mesozoic-Cenozoic exhumation history of Northern Svalbard and its regional significance: Constraints from apatite fission track analysis,* Tectonophysics 514-517, 81-92

FALEIDE J.I., VDGNES E., GUDLAUGSSON S.T., 1993 L*ate Mesozoic-Cenozoic evolution of the south-western Barents Sea in a regional rift-shear tectonic setting,* Marine and Petroleum Geology, vol 10, p.186-214

FALEIDE J.I., TSIKALAS F., BREIVIK A.J.,MJELDE R.,RITZMANN O., ENGEN Ø., WILSON J., ELDHOLM O., 2008 *Structure and evolution of the continental margin off Norway and the Barents Sea,* Episodes, vol.31, no.1

FARLEY K.A. 2002 *(U-Th)/He Dating: Techniques, Calibrations, and Applications,* Rev. Min. Geochem. 47, pp. 819–824

Final well report: 7220/10-1, 2012, ENI Norge

GABRIELSEN R.H., FŒRESETH R.B., JENSEN L.N., KALHEIM J.E., RIIS F., 1990 *Structural elements of the Norwegian continental shelf. Part I: the Barents Sea Region,* NPD Bulletin n.6

GLØRSTAD-CLARK E., FALEIDE J.I., LUNDSCHIEN B.A., NYSTUEN J.P., 2010 *Triassic seismic sequence stratigraphy and paleogeography of the western Barents Sea area,* Marine and Petroleum Geology, 27, 1448-1475

GLØRSTAD-CLARK E., BIRKELAND E.P., NYSTUEN J.P., FALEIDE J.I., MIDTKANDAL I., 2011 *Triassic platform-margin deltas in the western Barents Sea,* Marine and Petroleum Geology, 28, 1294-1314

GREEN P. F., DUDDY I. R., 2010 *Synchronous exhumation events around the Arctic including examples from Barents Sea and Alaska North Slope*, Petroleum Geology: From Mature Basins to New Frontiers – Proceedings of the 7th Petroleum Geology Conference, 633–644

HOCHULI P.A., VIGRAN J.O., 2010 *Climate variation in the Boreal Triassic – Inferred from palynological record from the Barents Sea,* Palaeogeography, Palaeoclimatology, Palaeoecology 290, 20–42

Havis discovery evaluation report, 2012, Statoil

HENRIKSEN E., RYSETH A.E., LARSSEN G.B., HEIDE T., RØNNING K., SOLLID K., STOUPAKOVA A.V., 2011 *Tectonostratigraphy of the greater Barents Sea: implications for petroleum systems,* Arctic Petroleum Geology. Geological Society, London, Memoirs, 35, 163–195

KETCHAM, R.A., 2005, *Forward and inverse modelling of low-temperature thermochronology data*, Rev. Mineral. Geochem. 58, 275–314

KETCHAM R.A., 2013 *HeFTy Version 1.8.1.*, PhD Thesis

LABERG J.S., ANDREASSEN K.,VORREN T.O., 2012 *Late Cenozoic erosion of the high-latitude southwestern Barents Sea shelf revisited,* GSA Bulletin, vol. 124; no. 1/2; p.77–88

REINERS P.W., BRANDON M., 2006 *Using Thermochronology to Understand Orogenic Erosion,* Annu. Rev. Earth Planet. Sci.34:419-466

www.npd.no

APPENDIX

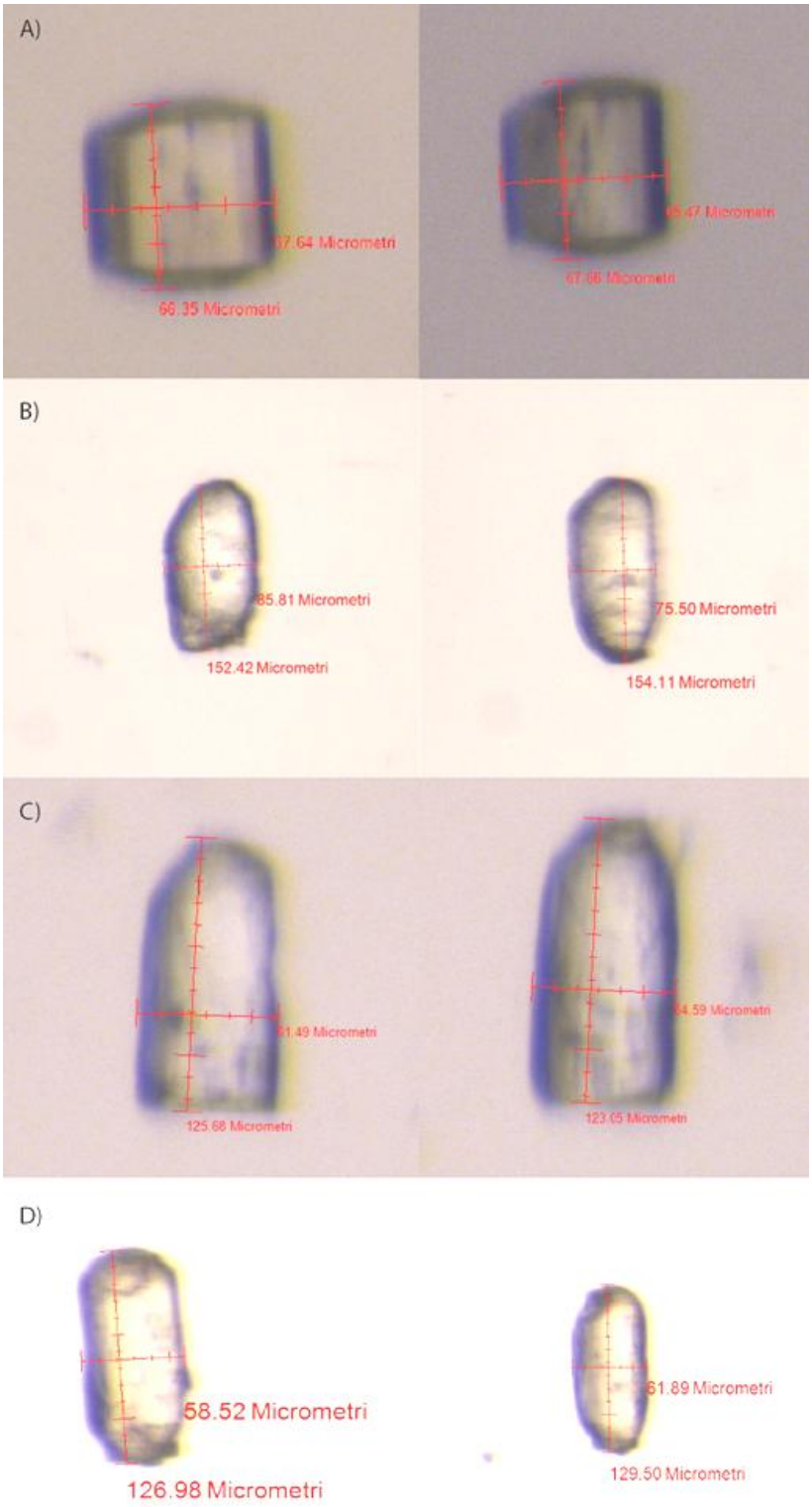
A)
67.64 Micrometri
66.35 Micrometri
67.66 Micrometri
B)
85.81 Micrometri
152.42 Micrometri
75.50 Micrometri
154.11 Micrometri
C)
125.68 Micrometri
123.05 Micrometri
D)
58.52 Micrometri
126.98 Micrometri
61.89 Micrometri
129.50 Micrometri

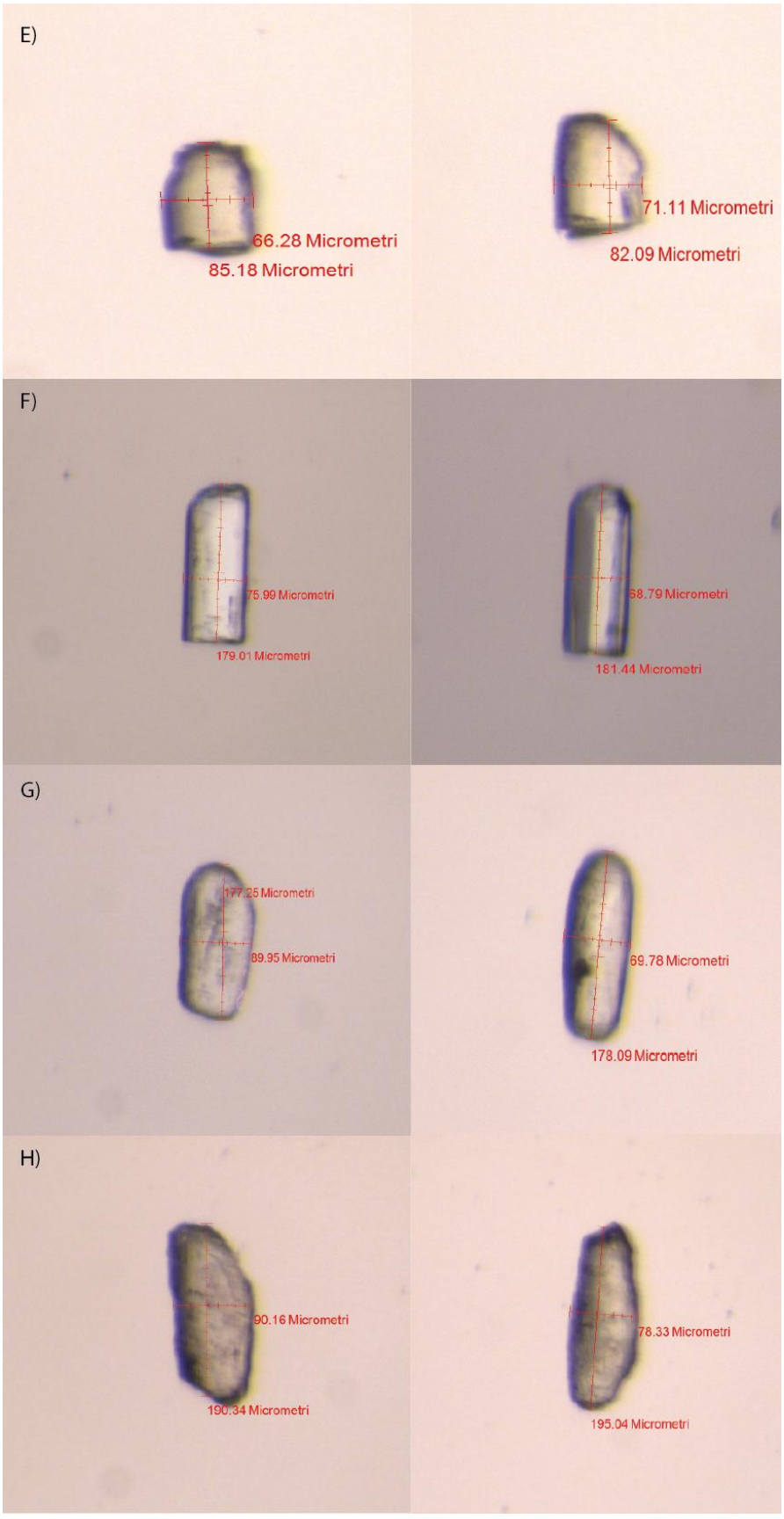
E)
66.28 Micrometri
85.18 Micrometri
71.11 Micrometri
82.09 Micrometri
F)
75.99 Micrometri
179.01 Micrometri
68.79 Micrometri
181.44 Micrometri
G)
177.25 Micrometri
89.95 Micrometri
69.78 Micrometri
178.09 Micrometri
H)
90.16 Micrometri
190.34 Micrometri
78.33 Micrometri
195.04 Micrometri

I)

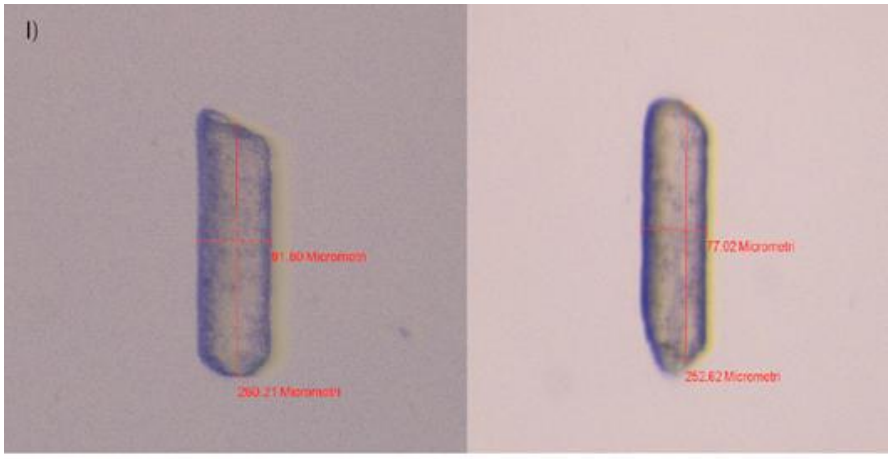
91.80 Micrometri
260.21 Micrometri
77.02 Micrometri
252.62 Micrometri

J)


90.10 Micrometri
155.52 Micrometri
85.26 Micrometri
157.47 Micrometri

K)


95.50 Micrometri
195.40 Micrometri
84.84 Micrometri
199.09 Micrometri

L)

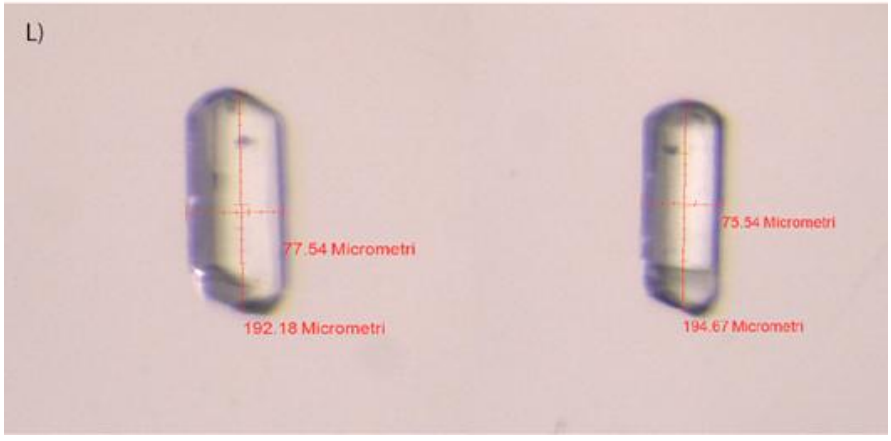
77.54 Micrometri
192.18 Micrometri
75.54 Micrometri
194.67 Micrometri

M)

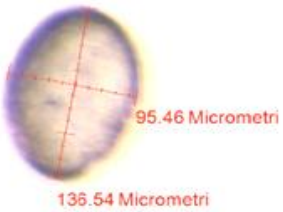
95.46 Micrometri
136.54 Micrometri

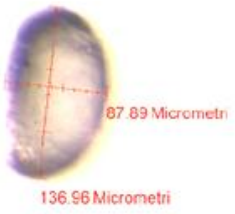
87.89 Micrometri
136.96 Micrometri

N)

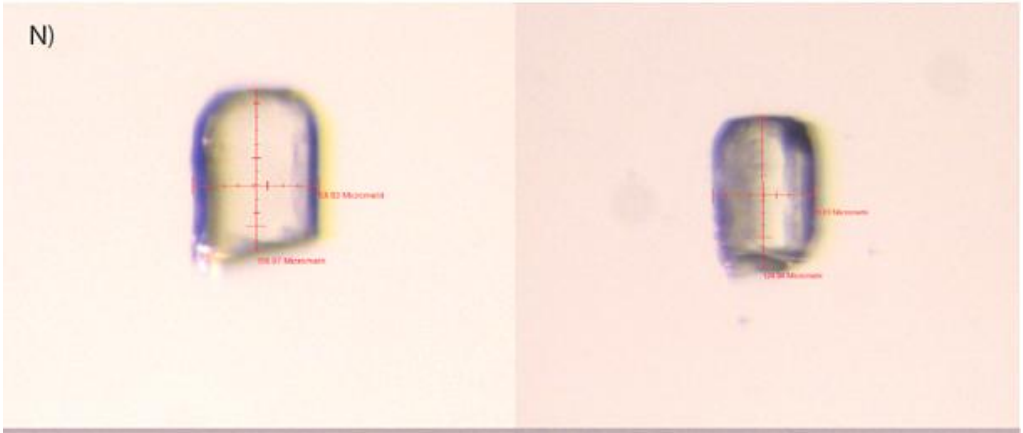

O)

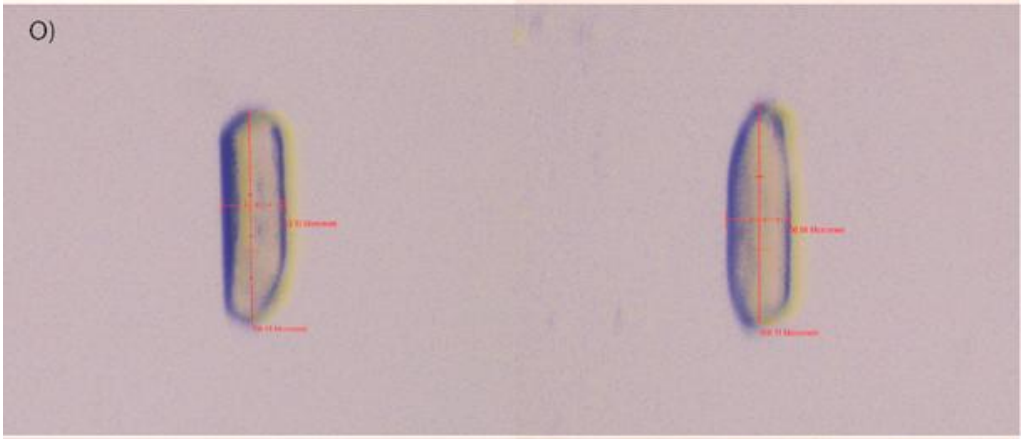

P)

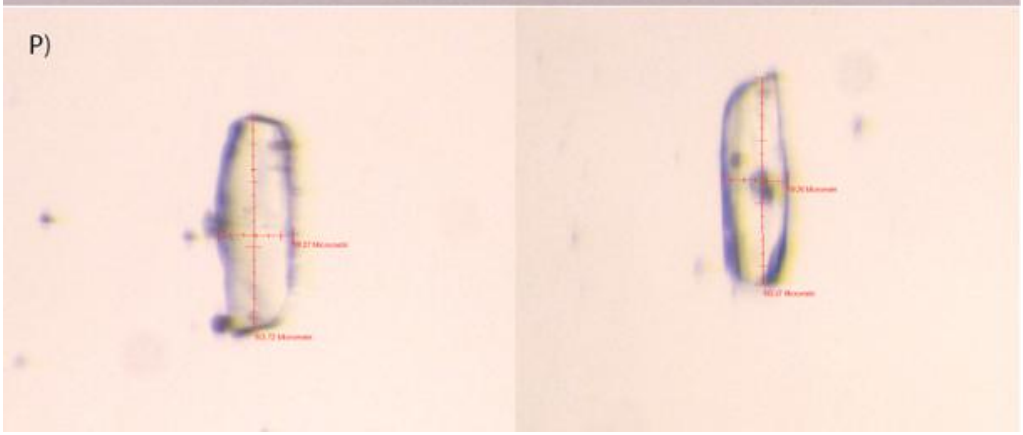

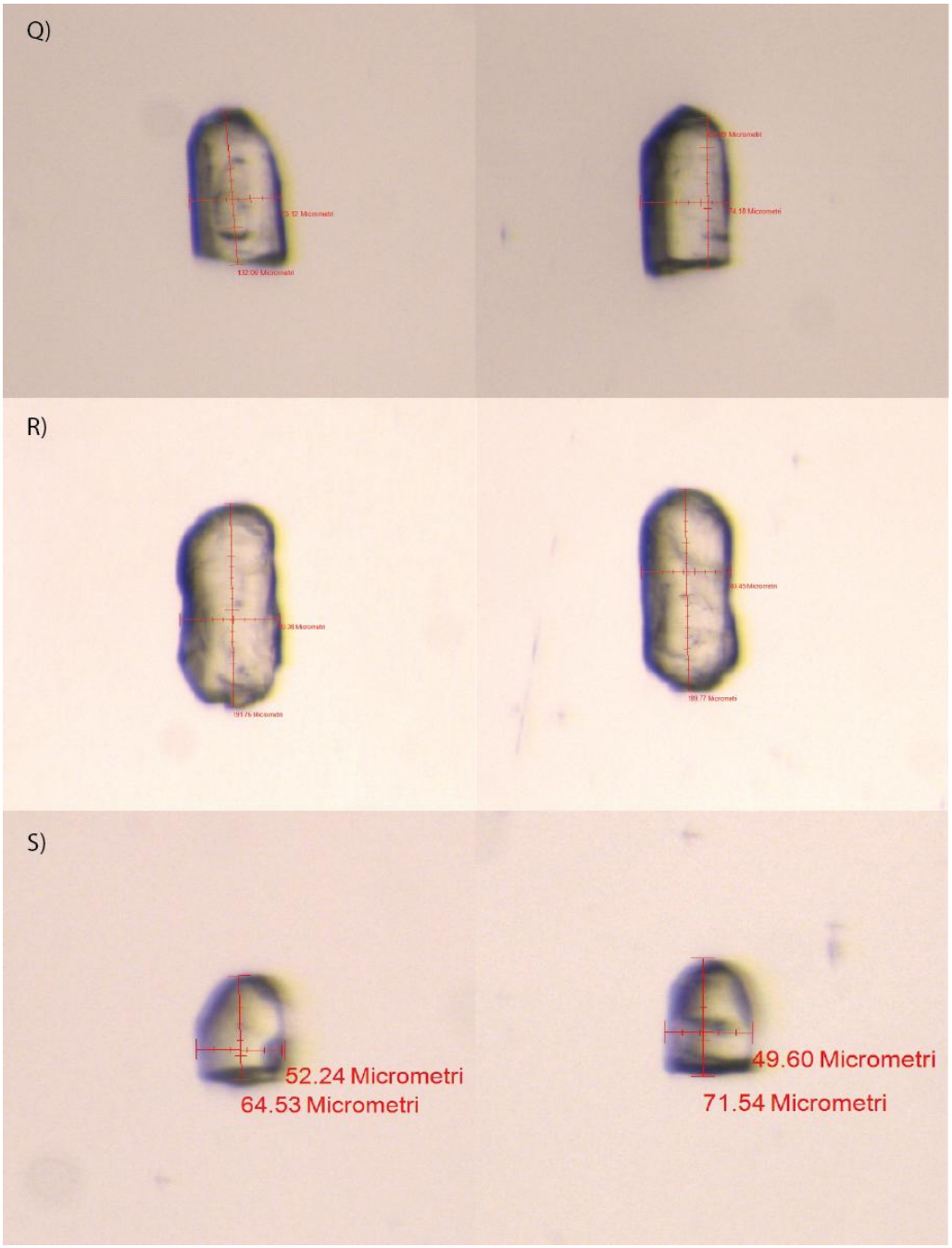

Tables . The photos in the appendix shows all the crystals collected for this work. Each one is characterised by two photos parallel to the c axis and perpendicular alternatively to the a axis and b axis. A) *HA1_1* B) *HA5_1* C) *HA6_1* D) *HA9_1* E) *HA9_2* F) *SL2_1* G) *SL2_2* H) *SL2_3* I) *SL5_1* J) *SL5_2* K) *SL5_3* L) *SL5_4* M) *SL5_5* N) *SL6_1* O) *SL6_2* P) *SL6_3* Q) *SL6_4* R) *SL6_5* S) *SL7_1*